STELLAR SURFACE AS LOW-RANK MODIFICATION IN ITERATIVE METHODS FOR BINARY NEUTRON STARS

STEPHEN R. LAU

Abstract. We present a new multidomain spectral method for the treatment of nonspherical stellar surfaces in iterative methods for binary neutron stars. A stellar surface changes throughout the course of an iterative solution, potentially stalling the convergence. Our method affords low-complexity updates of the relevant subdomain preconditioners, thereby avoiding such stalling. Unlike current collocation (or nodal) approaches for treating surfaces (which rely on coordinate transformations to ensure that stellar surfaces arise at subdomain boundaries), our approach requires no regridding or nontrivial Jacobians. For polytropes with an equation of state specified by an integer polytropic index, our method delivers exponential accuracy with increased truncation, although for "stiff" equations of state (e.g. fractional) it suffers from the same accuracy loss as current methods. We have presented an outline of our approach before, but here present details with numerical tests.

1. Introduction

We present a strategy for the treatment of nonspherical stellar surfaces when numerically constructing binary neutron stars (BNS). Our strategy, based on modal spectral methods, is likely broadly applicable. For example, it could serve as a component in solving, via conformal methods [1, 2, 3, 4], the constraint equations of general relativity for binary neutron star initial data (and possibly blackhole initial data with apparent horizon boundary conditions). Nonetheless, our own goal is the construction of helically symmetric BNS solutions (exact, excluding numerical error) to the matter-Einstein equations; see further remarks in Subsection 1.2. This paper focuses on the construction of equilibrium configurations in Newtonian theory, a benchmark problem [5, 6, 7, 8] which advances us towards our longer-term goal and a stage for presenting our general strategy. While this paper only considers circular orbits and polytropic equations of state, we do not believe our approach to stellar surfaces is limited by either assumption. The central ideas of our approach have appeared before [9]. However, this paper goes beyond that account both in addressing technical details and performing numerical tests.

The key difference between our work and similar earlier approaches (described in the next subsection) is that we adopt modal spectral methods, both to achieve sparse systems of equations and because of preconditioning issues. As a second longer-term goal, we seek to exploit the sparsity associated with our modal approach, thereby achieving quantifiably fast solvers for gravitational initial data. Work towards this second goal is also incomplete. Our modal approach has been spelled out in [10, 11, 12]. While we sketch some of the key features, we do not repeat details here. Our focus is on the new development: low-rank treatment of the stellar surfaces. Nonetheless, another novelty of this work is its further development of modal spectral methods for BNS problems.

Corresponding author: S. R. Lau. Email: lau@math.unm.edu.

The problem of constructing (and evolving) fluid stars is not dissimilar to other problems involving fluid interfaces. Irregular interfaces and possible loss of smoothness thereon arise in myriad fluid and solid mechanical applications, for example interfacial flows involving drops and bubbles; see e.g. [13, 14]. Interest often lies with the interface dynamics, as governed by the Navier Stokes equations subject to inclusion of (singular) surface-tension forces. However, many problems in applied fluids are well-approximated by Stokes flow, for which integral formulations are well-developed; see the discussions in [15, 16, 17]. A Poisson-type problem describes Stokes flow (however interfaces are treated); likewise, the Poisson equation features prominently in this work, although its origins are different. Here it arises through inclusion of gravitational forces in the nonrelativistic Euler equations.

Numerical methods for addressing interface problems are likewise manifold, and an exhaustive review is not possible. Nonetheless, our treatment of stellar surfaces is (in concept, if not in details) reminscient of "domain embedding methods"; see, for example, [18, 19, 20, 21]. These methods focus on, for example, elliptic PDE problems posed on irregular shaped domains. The idea is to embed the irregular domain within a simpler computational domain, such as a rectangular box or sphere. Such an embedding proves advantageous when well-known solution methods (i.e. integral representations and/or fast numerical techniques) are available for the simpler domain. The challenge is then to treat the physical boundary which now arises as an irregular surface inside the computational domain. Similar issues arise when the coefficients defining an elliptic PDE are discontinuous on irregular surfaces within a computational domain. The Immersed Interface Method [22, 23] addresses both kinds of problems. Ref. [24] presents recent work on such problems, and it gives a more comprehensive literature review.

In what remains of this introduction, we (1) overview numerical methods for BNS initial data, (2) more fully describe our own first goal, and (3) outline the sections of this paper.

1.1. **Overview of numerical methods for BNS initial data.** Recent BNS evolutions start with initial data constructed via one of two approaches. The first approach stems from methods introduced by J. W. York, both in its original form [1, 2] and in a 1999 reworking partly with H. P. Pfeiffer known as the *conformal thin sandwich (CTS) method* [3, 4]. The second approach yields *Meudon data* [25, 26, 27], named after its developing group. In principle, it yields a complete solution to Einstein's equations, rather than just initial data.

A number of codes are now capable of generating BNS initial data for the combined matter-Einstein equations, a problem considerably more challenging than the test problems considered here. These codes are reviewed in [28], and the following is based in part on that review. The Princeton-group code described in [29] relies on AMR and the multigrid technique. The BAM code [30] also has a multigrid solver, one relying on nested boxes and Gauss-Seidel relaxation. The recent COCAL code [31] features coordinate patches on which appropriate Green's function expansions are exploited to solve relevant Poisson-type nonlinear equations. The remaining codes, discussed now, are based on nodal spectral methods.

To our knowledge, the first work on spectral methods with GR applications in mind appeared in the proceedings of ICOSAHOM 95 [32].[1] Ultimately, the ideas presented in that volume were developed [25, 26, 27] and incorporated into the LORENE code [34] for solving BNS problems. LORENE is a multidomain collocation code based on two nested sets of subdomains, each a family of (at least two) concentric spherical shells with a center-filling

[1]The fundamental reference [33] on "integration preconditioning", the basis for our own work, appears in the same volume.

ball. One set of subdomains is associated with each star. Although this configuration involves significant subdomain overlap, it is a strikingly simple solution to the nontrivial geometry associated with BNS problems. Using a variant of the self-consistent field method described below, the LORENE code solves the helically symmetric Einstein equations subject to a conformal-flatness assumption.

The Simulating Extreme Spacetimes (SXS) project [35], with key groups at Cornell, Caltech, CITA, and CSU Fullerton (and elsewhere), has also adopted spectral methods to model binary inspiral and merger. Indeed, the Spectral Einstein Code (SpEC) [36] —developed chiefly by L. Kidder, H. Pfeiffer, and M. Scheel— also makes use of multidomain collocation methods. In particular, Pfeiffer's EllipticSolver module [37] within SpEC involves covering the spacetime surrounding two neutron stars (say) with a complicated arrangement of blocks, spherical shells, and cylindrical shells. Coupled elliptic systems of PDE posed on such a domain are then solved using iterative methods (typically GMRES) with a finite-difference preconditioning employed for efficiency and accuracy. For our own work we have made direct use of the domain decomposition used by SpEC's EllipticSolver. Descriptions of BNS initial data generated with SpEC appear in [38, 39, 40].

The SGRID code [41, 42, 28] also relies on nodal spectral methods, along with a novel approach for covering the computational domain developed in particular by Tichy [41]. The approach features coordinate patches surrounding each compact object similar to those introduced by Ansorg [43], rather than the spherical domains used in LORENE and SpEC. The basis functions corresponding to these patches are tensor products of two Chebyshev polynomials and one trigonometric polynomial, that is a double-Chebyshev/Fourier basis.

Insofar as the treatment of stellar surfaces is concerned, the LORENE, SpEC, and SGRID projects employ coordinate mappings to distort (spherical, spherical shell, or patch) subdomains in order that the stellar surface arises precisely as a subdomain interface. Such mapping ameliorates the Gibb's phenomena, although achieving "spectral convergence" for "stiff" equations of state is (in our understanding) still an open problem. Moreover, distortion of the subdomain necessitates regridding, thereby introducing non-trivial Jacobians and changing the bulk operators. As a result, preconditioner recomputation at each iteration stage may be necessary to prevent stalling of the adopted iterative method.

1.2. **Helically symmetric BNS spacetimes.** Our own goal is numerical construction of helically symmetric spacetimes describing binary neutron stars, a goal nearly identical to the one already carried out in the Meudon program. The essential theoretical differences are that we (i) adopt a field decomposition in terms of "helical scalars" (essentially the Laudau-Lifshitz formalism [44]) rather than the standard 3+1 formalism [1], and (ii) we intend to make no use of the *Ansatz* of conformal flatness. Even still, since they are devoid of inspiral, the solutions that we seek are ultimately unphysical. While helically symmetric solutions of the non-vacuum Einstein equations would be of interest in their own right (for example, from the standpoint of their asymptotic structure), our interest lies with using them to define improved trial data for the conformal thin sandwich equations.

1.3. **Outline.** This paper is organized as follows. Section 2 considers the model problem of a spherically symmetric single star, that is a Lane Emden star. This simple model showcases the key ideas behind both our modal spectral methods and how they are used to treat stellar surfaces. Section 3 describes the Newtonian BNS problem, and our numerical methods for solving it. While summarizing some material from [11], it mostly focuses on the technical

issues associated with our treatment of stellar surfaces, in particular how a surface is realized within the overall system of equations defining our approximation of the Newtonian problem. In Section 3 we also discuss to role of preconditioning as it pertains to stellar surfaces which evolve during iterative solution of the problem. We address complexity issues associated with updating the preconditioner as the surface evolves. Finally, Section 3 also briefly reviews the self-consistent-field (SCF) method, and the particular way we have used it to solve the Newtonian problem. Section 4 documents the results of numerical experiments testing our approach. Finally, appendices present further details left out of the main text. In particular, Appendix C presents the full details of how we treat stellar surfaces through "tau-conditions", a defining feature of modal spectral methods based on "integration preconditioning". These details also appeared in [9].

2. Model problem

This section describes our model problem: construction of a spherically symmetric Newtonian star, a Lane-Emden polytrope. Our aim here is to fix ideas and describe in a simple context the key aspects of our numerical approach to binary stars. We view the following as fixed constants: G, strength of gravity; n, polytropic index in the equation of state (EOS); K, constant in the EOS. The polytropic EOS $p = K\rho^{1+1/n}$ (for now with $n > 0$) relates the pressure p to the density ρ. These constants fix the "theory" of gravity and matter. With this viewpoint, a stellar model is determined by a single piece of data: $\rho_{\rm c}$, the central density of the star.

Our domain is the interval $[0, r_{\rm out}]$, where $r_{\rm out}$ is the outer radius. On this interval we consider the following unknown quantities (to be solved for): (i) the stellar enthalpy function $h(r) = K(1+n)\rho^{1/n}(r)$ and (ii) a scalar κ. Here the situation is analogous to the binary problem considered later, where the unknowns will again be the enthalpy plus auxiliary "constants". The location $R < r_{\rm out}$ of the stellar surface is also unknown a priori. Nonetheless, $h(r) = 0 = \rho(r)$ for $r \geq R$; whence we view R as determined by h. These unknowns are subject to the following problem:

$$L\Phi = 4\pi G\rho(r) \text{ for } 0 < r < r_{\rm out}, \quad \Phi'(0) = 0, \quad \Phi'(r_{\rm out}) = -\Phi(r_{\rm out})/r_{\rm out} \tag{1a}$$

$$\kappa = h(r) + \Phi(r) \text{ for } 0 \leq r \leq R \tag{1b}$$

$$h(0) = K(1+n)\rho_c^{1/n}. \tag{1c}$$

Here $L\Phi \equiv r^{-2}(r^2\Phi')'$, with a prime denoting differentiation in r, is the radial Laplacian, and the constancy of $\kappa = h(r) + \Phi(r)$ balances the chemical and gravitational potentials. The solution

$$h(r) = \begin{cases} 2K\rho_{\rm c}(\pi r/R)^{-1}\sin(\pi r/R) & \text{for } 0 \leq r \leq R \\ 0 & \text{for } r \geq R \end{cases} \tag{2a}$$

$$\kappa = -2K\rho_{\rm c}, \tag{2b}$$

where $R = \sqrt{K\pi/(2G)}$, solves (1) for the choice $n = 1$. Here we view the gravitational potential and density,

$$\Phi(r) = \begin{cases} -2K\rho_{\rm c}\big[1 + (\pi r/R)^{-1}\sin(\pi r/R)\big] & \text{for } 0 \le r \le R \\ -2K\rho_{\rm c}R/r & \text{for } r \ge R \end{cases} \tag{3a}$$

$$\rho(r) = \begin{cases} \rho_{\rm c}(\pi r/R)^{-1}\sin(\pi r/R) & \text{for } 0 \le r \le R \\ 0 & \text{for } r \ge R, \end{cases} \tag{3b}$$

as quantities determined by the enthalpy h. The density ρ is recovered trivially, and the gravitational potential Φ through solution of the Poisson problem from (1).

2.1. **Formulas for Chebyshev polynomials on a generic interval.** This subsection collects various formulas involving Chebyshev polynomials on a generic interval $\mathsf{D} \equiv [r_{\min}, r_{\max}]$. With these formulas in hand, the next subsection describes our numerical method for solving the problem (1). Let $\mathbf{T}(\xi) = [T_0(\xi), T_1(\xi), T_2(\xi), \dots]$ represent an infinite row of Chebyshev values. Then we have the following identities

$$\xi\mathbf{T}(\xi) = \mathbf{T}(\xi)\mathsf{A} \tag{4a}$$

$$\xi^2\mathbf{T}(\xi) = \mathbf{T}(\xi)\mathsf{A}^2 \tag{4b}$$

$$\mathbf{T}(\xi) = \mathbf{T}'(\xi)\mathsf{B}_{[1]} \tag{4c}$$

$$\mathbf{T}(\xi) = \mathbf{T}''(\xi)\mathsf{B}_{[2]}^2, \tag{4d}$$

where the banded matrices [33, 45] A (tridiagonal), A^2 (pentadiagonal), $\mathsf{B}_{[1]}$ (tridiagonal), and $\mathsf{B}_{[2]}^2$ (pentadiagonal) are of infinite size; see Appendix A. San serif font will be used for infinite-sized matrices, and regular font for their finite truncations. Here the subscripts [1] and [2] indicate the number of leading rows with all zeros as entries. Suppose that $\widetilde{\boldsymbol{f}} = (\widetilde{f}_0, \widetilde{f}_1, \widetilde{f}_2, \cdots)^T$ are the Chebyshev coefficients for a function f, that is formally $f(\xi) = \sum_{k=0}^{\infty} \widetilde{f}_k T_k(\xi)$. Then, for example, the third relationship in (4) implies that $\mathsf{B}_{[1]}\widetilde{\boldsymbol{f}}$ are the Chebyshev coefficients for an antiderivative F of f such that $\widetilde{F}_0 = 0$.

To collect formulas for the generic interval D rather than the standard interval $[-1, 1]$, define the mapping

$$\xi(r) \equiv \lambda^{-1}(r - \bar{r}), \qquad \lambda^{-1} \equiv \frac{2}{r_{\max} - r_{\min}}, \qquad \bar{r} \equiv \frac{1}{2}(r_{\min} + r_{\max}). \tag{5}$$

Then we set $\mathsf{B}_{r[1]} \equiv \lambda\mathsf{B}_{[1]}$, $\mathsf{B}_{r[2]}^2 \equiv \lambda^2\mathsf{B}_{[2]}^2$, $\mathsf{A}_r \equiv \lambda\mathsf{A} + \bar{r}\mathsf{I}$, and $\mathsf{A}_r^2 \equiv \lambda^2\mathsf{A}^2 + 2\lambda\bar{r}\mathsf{A} + \bar{r}^2\mathsf{I}$, where I is the infinite-size identity matrix and the subscript r serves to distinguish these matrices from those associated with the standard interval $[-1, 1]$. For D the formulas corresponding to (4) are

$$r\mathbf{T}(\xi(r)) = \mathbf{T}(\xi(r))\mathsf{A}_r \tag{6a}$$

$$r^2\mathbf{T}(\xi(r)) = \mathbf{T}(\xi(r))\mathsf{A}_r^2 \tag{6b}$$

$$\mathbf{T}(\xi(r)) = \frac{d}{dr}\mathbf{T}(\xi(r))\mathsf{B}_{r[1]} \tag{6c}$$

$$\mathbf{T}(\xi(r)) = \frac{d^2}{dr^2}\mathbf{T}(\xi(r))\mathsf{B}_{r[2]}^2. \tag{6d}$$

These formulas yield interpretations for the actions of the matrices A_r, A_r^2, $\mathsf{B}_{r[1]}$, and $\mathsf{B}_{r[2]}^2$ when acting on coefficient vectors $\widetilde{\boldsymbol{f}}$. Now $\widetilde{\boldsymbol{f}}$ is associated with modal expansions of a function $f(r) = \sum_{k=0}^{\infty} \widetilde{f}_k T_k(\xi(r))$ defined on D.

2.2. **Poisson problem on a single interval D.** Our interest lies with approximation of the model problem, for which we will adopt two overlapping subintervals. To set the stage for that approximation, here we consider the (spherical) Poisson problem on a single interval. We first define Dirichlet and Neumann vectors:

$$\boldsymbol{\delta}(r) = [T_0(\xi(r)), T_1(\xi(r)), T_2(\xi(r)), \ldots, T_N(\xi(r))] \tag{7a}$$

$$\boldsymbol{\nu}(r) = [0, T_1'(\xi(r)), T_2'(\xi(r)), \ldots, T_N'(\xi(r))]\lambda^{-1}, \tag{7b}$$

where primes indicate differentiation in argument. Note that here we consider finite-length row vectors based on a truncation N. These vectors will be used to enforce boundary conditions. Next, we write the Poisson equation above as

$$\frac{d^2}{dr^2}\Big(r^2\Phi\Big) - 2\frac{d}{dr}\Big(r\Phi\Big) = 4\pi G r^2 \rho(r). \tag{8}$$

We then introduce (finite-size) modal-coefficient vectors $\widetilde{\boldsymbol{\Phi}}$ and $\widetilde{\boldsymbol{\rho}}$, such that

$$\mathcal{P}_N\Phi(r) = \sum_{k=0}^{N} \widetilde{\Phi}_k T_k(\xi(r)), \qquad \mathcal{P}_N\rho(r) = \sum_{k=0}^{N} \widetilde{\rho}_k T_k(\xi(r)) \tag{9}$$

respectively approximate the potential and density. These vectors obey

$$\big(I_{[2]}A_r^2 - 2B_{r[2]}A_r\big)\widetilde{\boldsymbol{\Phi}} = 4\pi G B_{r[2]}^2 A_r^2 \widetilde{\boldsymbol{\rho}}, \tag{10}$$

our spectral approximation of the Poisson equation which, thus far, ignores boundary conditions. Notice that (10) corresponds to two integrations of (8). In terms of colon notation, the matrices in (10) are the truncations

$$\begin{aligned} A_r^2 &= \mathsf{A}_r^2(0{:}N,0{:}N) \\ B_{r[2]}A_r &= \mathsf{B}_{r[2]}(0{:}N,{:})\mathsf{A}_r({:},0{:}N) \\ B_{r[2]}^2A_r^2 &= \mathsf{B}_{r[2]}^2(0{:}N,{:})\mathsf{A}_r^2({:},0{:}N). \end{aligned} \tag{11}$$

Note (i) our use of Roman and san serif fonts to distinguish between finite-size and infinite-size matrices and (ii) that there is no issue with implied infinite summations here, since each infinite-size matrix is banded. For future use we further define

$$\mathcal{BL} \equiv \big(I_{[2]}A_r^2 - 2B_{r[2]}A_r\big)(2{:}N). \tag{12}$$

Here $\mathcal{BL}$ has dimensions $(N-1)\times(N+1)$, and results from stripping off the first two rows of zeros from $I_{[2]}A_r^2 - 2B_{r[2]}A_r$. Then, for example, an approximation of (10) with Dirichlet boundary conditions (not the correct boundary conditions for our problem) would be

$$\begin{pmatrix} \delta(r_{\min}) \\ \delta(r_{\max}) \\ \mathcal{BL} \end{pmatrix} \widetilde{\boldsymbol{\Phi}} = 4\pi G B_{r[2]}^2 A_r^2 \widetilde{\boldsymbol{\rho}} + \Phi(r_{\min})\mathbf{e}_0 + \Phi(r_{\max})\mathbf{e}_1, \tag{13}$$

where $\mathbf{e}_0, \mathbf{e}_1 \in \mathbb{R}^{(N+1)\times 1}$ are the first two canonical basis vectors.

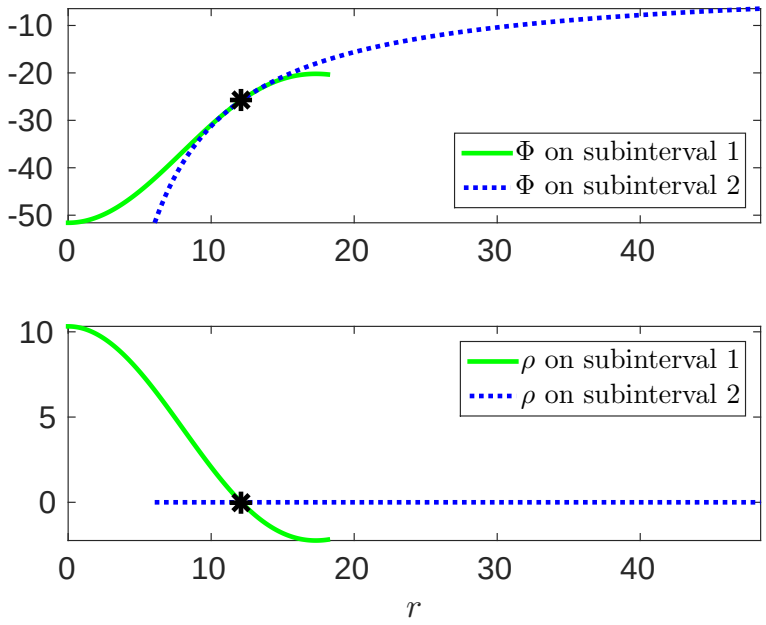

FIGURE 1. LANE-EMDEN STAR SOLUTION. The blue dotted curves depict the solution on D^2, while the green solid line the solution on D^1. The black asterisk corresponds the stellar surface $r = R$; this point lies in $\mathsf{D}^1 \bigcap \mathsf{D}^2$.

2.3. **Numerical approximation of the model problem.** We partition the domain into two overlapping subintervals:[2] $\mathsf{D}^1 = [0, r_{\max}]$ and $\mathsf{D}^2 = [r_{\min}, r_{\text{out}}]$, where we assume that we have been lucky enough to ensure $r_{\min} < R < r_{\max}$. Whilst comparing with the last subsection's formulas, please notice that "$r_{\min}$" and "$r_{\max}$" for D^1 are 0 and $r_{\max}$, whereas the "$r_{\min}$" and "$r_{\max}$" for D^2 are $r_{\min}$ and r_{out}. Respectively, the mappings between $[-1, 1]$ and the subintervals D^1 and D^2 are

$$\begin{aligned} \xi^1(r) &= \frac{2r - r_{\max}}{r_{\max}} \\ \xi^2(r) &= \frac{2r - r_{\text{out}} - r_{\min}}{r_{\text{out}} - r_{\min}}. \end{aligned} \tag{14}$$

2.3.1. *Approximation of the Poisson problem.* Our approximation on the coupled subintervals involves the system matrix

$$\mathcal{M}(R) = \left[\begin{array}{c|c} \mathcal{M}(R)^{11} & \mathcal{M}(R)^{12} \\ \hline \mathcal{M}(R)^{21} & \mathcal{M}(R)^{22} \end{array}\right] \equiv \left[\begin{array}{c|c} \boldsymbol{\nu}^1(0) & \mathbf{0} \\ \boldsymbol{\delta}^1(R) & -\boldsymbol{\delta}^2(R) \\ \mathcal{BL}^1 & \mathbf{0} \\ \hline -\boldsymbol{\nu}^1(R) & \boldsymbol{\nu}^2(R) \\ \mathbf{0} & \boldsymbol{\nu}^2(r_{\text{out}}) + r_{\text{out}}^{-1}\boldsymbol{\delta}^2(r_{\text{out}}) \\ \mathbf{0} & \mathcal{BL}^2 \end{array}\right] \tag{15}$$

[2]Throughout, superscript indices refer to the subintervals; in particular a superscript 2 most always refers to the second subdomain D^2 and not squaring. However, on both intervals we continue to use A_r^2 and $A_r^2 B_{r[2]}^2$ for the matrices considered earlier.

and the corresponding right-hand side

$$\boldsymbol{g} \equiv \begin{bmatrix} 0 \\ 0 \\ 4\pi G\mathcal{B}\widetilde{\boldsymbol{\rho}}^1 \\ 0 \\ 0 \\ \mathbf{0} \end{bmatrix}, \tag{16}$$

where $\mathcal{B}\widetilde{\boldsymbol{\rho}}^1 \equiv (B^2_{r[2]}A^2_r\widetilde{\boldsymbol{\rho}}^1)(2{:}N^1)$. Provided that we know the value of R in advance, the solution $\widetilde{\boldsymbol{\Phi}} \equiv (\widetilde{\boldsymbol{\Phi}}^1; \widetilde{\boldsymbol{\Phi}}^2)$ to the Poisson problem then obeys $\mathcal{M}(R)\widetilde{\boldsymbol{\Phi}} = \boldsymbol{g}$. Finally, we remark the while the matrix $\mathcal{M}(R)$ has many rows, visually it has six rows (of course some of these rows are in fact matrices). In this view, the first, second, fourth, and fifth rows express the *tau-conditions*, reflecting both boundary and matching conditions. The matching conditions are enforced by the second and fourth rows.

2.3.2. *Iterative method.* We adopt the *self-consistent field (SCF) method* for solving our spectral approximation of the problem. In our view, the SCF method is a fixed-point procedure for the enthalpy, represented by its spectral expansion coefficients $\widetilde{\boldsymbol{h}}^1$ on D^1, and the scalar κ. **Algorithm 1** presents a single fixed-point iteration.

Algorithm 1 SCF ITERATION. Input is $(\widetilde{\boldsymbol{h}}^1, \kappa)$, which includes the modal coefficient vector $\widetilde{\boldsymbol{h}}^1$ for the enthalpy on D^1. Output is the new $(\widetilde{\boldsymbol{h}}^1, \kappa)$.

1: Find the root R of $\mathcal{P}_{N^1}h(r) = \sum_{k=0}^{N^1} \widetilde{h}^1_k T_k(\xi^1(r))$, say with bisection.
2: Perform a rank-2 update of the coefficient matrix $\mathcal{M}(R)$, ensuring that the matching tau-conditions correspond to the current R.
3: From $\widetilde{\boldsymbol{h}}^1$ form the density $\widetilde{\boldsymbol{\rho}}^1$, simply $\widetilde{\boldsymbol{\rho}}^1 = \frac{1}{2}K^{-1}\widetilde{\boldsymbol{h}}^1$ for $n = 1$.
4: Solve the described discrete Poisson problem $\mathcal{M}(R)\widetilde{\boldsymbol{\Phi}} = \boldsymbol{g}$.
5: Evaluate $\Phi_0 \equiv \sum_{k=0}^{N^1} \widetilde{\Phi}^1_k \delta^-_k$, and with it update $\kappa = K(n+1)\rho_{\mathrm{c}}^{1/n} + \Phi_0$.
6: Update the enthalpy via the potential equation: $\widetilde{h}^1_k = \kappa\delta_{0k} - \widetilde{\Phi}^1_k$ for $k = 0, 1, \ldots, N^1$.

2.4. **Numerical experiment.** This subsection describes an $n = 1$ computational experiment relying on the SCF method. Fix the physical parameters $K = 1.25$, $G = 0.0134$ and the model choice $\rho_{\mathrm{c}} = 10.32$, along with the domain choices

$$\mathsf{D}^1 = [r^1_{\min}, r^1_{\max}] = [0, \tfrac{3}{2}R], \qquad \mathsf{D}^2 = [r^2_{\min}, r^2_{\max}] = [\tfrac{1}{2}R, r_{\mathrm{out}}], \tag{17}$$

where $r_{\mathrm{out}} = 4R$. With these choices $R \simeq 12.105$, $r^2_{\min} \simeq 6.0525$, $r^1_{\max} \simeq 18.157$, and $r_{\mathrm{out}} \simeq 48.420$. Figure 1 depicts the associated Lane-Emden solution (3). Notice that on the overlap region $r^2_{\min} \le r \le r^1_{\max}$ the solution is double-valued. To make the plot, we have chosen the inner solution from (3) on D^1 (even beyond its validity interval), and the outer solution on D^2. In particular then, $\rho(r)$ takes negative values on D^1 for $r \in (R, r^1_{\max}]$. This Lane-Emden solution ($h = 2K\rho, \kappa$) defines the "exact" solution $(\widetilde{\boldsymbol{h}}^{1,\mathrm{exact}}, \kappa^{\mathrm{exact}})$ to our numerical problem, with $\widetilde{\boldsymbol{h}}^{1,\mathrm{exact}}$ the truncated Chebyshev spectrum of $h(r)$ on D^1.

Our SCF method requires an initial iterate $(\widetilde{\boldsymbol{h}}^{1,\mathrm{init}}, \kappa^{\mathrm{init}})$. We generate this as follows. First, we define a *different* Lane-Emden solution through the following reassignments: $G^{\mathrm{diff}} = 0.7G$

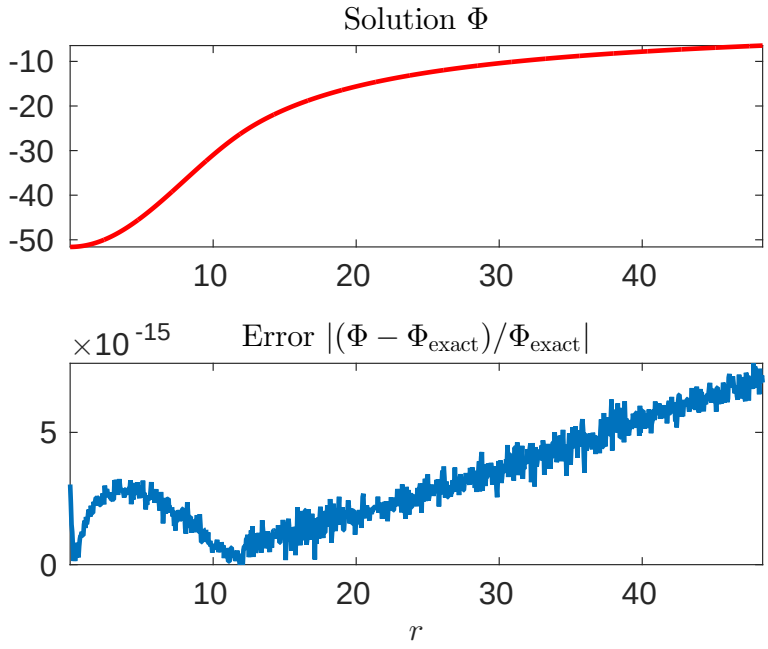

FIGURE 2. GRAVITATIONAL POTENTIAL DETERMINED BY THE SCF SOLUTION.

and $\rho_c^{\text{diff}} = 0.9\rho_c$. We then define

$$\kappa^{\text{init}} = -2K\rho_c^{\text{diff}}, \qquad h^{\text{init}}(r) = h^{\text{diff}}(r) + \gamma \sin\big(r(R^{\text{diff}} - r)\big), \qquad \gamma = 0.01. \tag{18}$$

With $N^1 = 50$ and $N^2 = 55$, the results of performing the SCF algorithm are then as follows.

q	err(h)	err(kappa)	kappa
1	2.27e-01	5.72e-01	-4.056269528953942e+01
2	5.17e-02	3.40e-02	-2.667730794617216e+01
3	3.04e-02	5.68e-02	-2.433452296773579e+01
4	1.71e-02	1.55e-02	-2.620102896893981e+01
5	4.30e-03	1.90e-03	-2.575098844900371e+01
6	6.78e-04	1.56e-04	-2.580402498850653e+01
7	7.55e-05	8.89e-06	-2.579977054426044e+01
8	6.32e-06	3.78e-07	-2.580009975545724e+01
9	4.15e-07	1.25e-08	-2.579999967817011e+01
10	2.20e-08	3.29e-10	-2.580000000849111e+01
11	9.64e-10	7.11e-12	-2.579999999981646e+01
12	3.55e-11	1.30e-13	-2.580000000000335e+01
13	1.12e-12	2.78e-14	-2.579999999999928e+01
14	4.43e-14	6.33e-15	-2.580000000000016e+01

The table lists the iteration number q, along with the relative errors $\|\widetilde{\boldsymbol{h}}^1 - \widetilde{\boldsymbol{h}}^{1,\text{exact}}\|_2 / \|\widetilde{\boldsymbol{h}}^{1,\text{exact}}\|_2$ and $|\kappa - \kappa^{\text{exact}}|/|\kappa^{\text{exact}}|$. The bisection step to find R from $\widetilde{\boldsymbol{h}}^1$ in **Algorithm 1** used a `1.0e-14` tolerance. Figure 2 depicts the corresponding numerical solution and error for the gravitational potential. To generate this plot, we have used interpolation onto a fine reference grid $\{r_k : k = 1, \ldots, N^{\text{ref}}\}$ with $N^{\text{ref}} = 1000$ points. In carry out this interpolation, we of course

use the inner solution $\widetilde{\mathbf{\Phi}}^1$ to obtain evaluations for points $r_k < R$ and the outer solution $\widetilde{\mathbf{\Phi}}^2$ to obtain evaluations for points $r_k > R$.

3. Binary problem

This section considers the problem of constructing a co-moving neutron star binary. We consider the Newtonian problem; Ref. [49] considers a generalization which includes waves based on the helically reduced wave equation (HRWE). We label one star I and the other II. More precisely, the stellar extents are determined by a stellar density $\rho(\mathbf{x})$ which is nonvanishing only on the interior $U = \{\mathbf{x} : \rho(\mathbf{x}) > 0\}$ of a compact set closure(U). The set $U = U_I \cup U_{II}$ is itself the union of two disjoint sets, one for each star. The boundaries ∂U_I and ∂U_{II} are the stellar surfaces and are a priori unknown, i.e. they are *free surfaces* in the problem. The "theory" of gravity and matter is set by the following fixed constants: G, strength of gravity; n, polytropic index; $K_{I,II}$, constant appearing in the stellar equation of state for star I, II. With this viewpoint, a Newtonian binary pair is determined by the following four choices: $\rho_{\max,I,II}$, maximum value of the density in star I, II; $\mathbf{x}_{I,II} = (0, 0, z_{I,II})$, location where maximum value $\rho_{\max,I,II}$ is realized. Here we have fixed the binary model with "Meudon choices"; see Subsection 3.4.

On the ball $\mathcal{D} \equiv \{\mathbf{x} : |\mathbf{x}| \leq r_{\rm out}\}$ we consider the following unknowns: (i) the stellar enthalpy $h(\mathbf{x}) \equiv K_{I,II}(n+1)\rho^{1/n}(\mathbf{x})$ and the scalars (ii,iii,iv,v) $\kappa_{I,II}, \Omega^2, \ell_z$. The aforementioned generalization [49] also has a fifth scalar ℓ_x as an unknown. The stellar surfaces are described by envelope functions $r_{I,II}(\boldsymbol{\theta}_{I,II})$ for the free surfaces $\partial U_{I,II}$. Here $\boldsymbol{\theta}_{I,II}$ are direction cosines relative to star I, II; i.e. $\boldsymbol{\theta} = (\sin\theta\cos\phi, \sin\theta\sin\phi, \cos\theta)$. Similar to the model problem, these surfaces are unknown a priori, but we view them as determined by the enthalpy. Whence, technically, they are not solved for. The stellar surfaces are zero sets of the enthalpy: $h(r_{I,II}(\boldsymbol{\theta}_{I,II})\boldsymbol{\theta}_{I,II}) = 0$. The unknowns are subject to the following equations: [cf. (1) and Ref. [27], both Eqs. (41,95) and page 11, second paragraph]

$$\nabla^2\Phi = 4\pi G\rho(\mathbf{x}), \qquad \mathcal{B}(\Phi) = 0 \tag{19a}$$

$$\kappa_{I,II} = h(\mathbf{x}) + \Phi(\mathbf{x}) - \tfrac{1}{2}\Omega^2\varpi^2(\mathbf{x}) \text{ for } \mathbf{x} \in U_I, U_{II} \tag{19b}$$

$$h(\mathbf{x}_{I,II}) = K_{I,II}(1+n)\rho^{1/n}_{\max,I,II}, \qquad \frac{\partial h_{I,II}}{\partial z}\Big|_{\mathbf{x}=\mathbf{x}_{I,II}} = 0. \tag{19c}$$

Here, $\mathcal{B}(\Phi) = 0$ is a nonlocal boundary condition (see **Remark 3.1** below), $\varpi^2(\mathbf{x}) := x^2 + (z-\ell_z)^2$ is the squared distance of a stellar fluid element from the rotation axis, and Ω is the rotation rate. The stars are assumed to lie on the z-axis, with the rotation axis (parallel to the y-axis) passing through $(0, \ell_z)$. Similar to the model problem, the constancy of $\kappa_{I,II}$ reflects a balance of chemical, gravitational, and (now also) rotational potential.

3.1. Domain decomposition and binary Poisson problem.

We adopt a multidomain spectral element approach for solving the binary problem, one based on sparse modal-tau methods [10, 11]. Here we concentrate on a Poisson problem, but our work also involves similar problems based on the HRWE. The problem domain $\mathcal{D}$ is viewed as a "2-center domain" and split into a collection of (overlapping and conforming) subdomains. The minimal configuration consists of the following 15 subdomains: blocks B^1, B^2, B^3, B^4, B^5; cylinders C^1, C^2, C^3, C^4, C^5; inner shells S^1_I, S^2_I around star I; inner shells S^1_{II}, S^2_{II} around star II; and an outer shell $S^1_{\rm out}$. Figure 3 depicts the decomposition. For binary problems

such domain decompositions were pioneered by Pfeiffer et al. [37] and play a key role in the `EllipticSolver` module of the Spectral Einstein Code [36].

Reference [11] has described our use of such decompositions in conjunction with sparse modal-tau methods. The details presented in that reference also pertain to the present work. In particular, we rely on the following results from [11].

- Sparse spectral representation of the Laplacian operator on blocks, cylinders, and shells. In this work we only give details for the Laplacian on shells. Refs. [11, 49] also consider the corresponding representation of the HRWE on these subdomains.
- "Gluing" of conforming and overlapping subdomains. As seen in Fig. 3, adjacent cylinders are conforming, whereas other subdomains, such as C^5 and B^5 overlap. Reference [11] examines how the gluing of subdomains is reflected in the overall linear system corresponding to a Poisson-type problem on $\mathcal{D}$.
- Preconditioning of the overall global solve. For a Poisson-type problem over $\mathcal{D}$ approximated by sparse modal-tau methods, Ref. [11] has addressed both the preconditioning of the bulk operator on each subdomain and the subdomain couplings. We mostly omit these details here, except insofar as they pertain to stellar surfaces.

One key difference between Ref. [11] and the present work concerns the nature of the 2-center domain. In [11] $\mathcal{D}$ was a "binary black-hole" (BBH) domain involving two inner excised regions; whereas here $\mathcal{D}$ is a "binary neutron star" (BNS) domain. Relative to a BBH domain, a BNS domain requires at least four extra subdomains both to fill in the regions where the stars lie and to handle the stellar surfaces. More precisely, shell J from [11] has been replaced by block B^2 and shells S^1_I, S^2_I. Likewise, shell H has been replaced by block B^4 and shells S^1_{II}, S^2_{II}. We have also renamed as $S^1_{\rm out}$ the outer shell O from [11]. Consider, for example, the B^2, S^1_I, S^2_I configuration surrounding the center $(0, 0, z_I)$. The block B^2 covers over the central "hole" of S^1_I, and the stellar surface ∂U_I will lie in the overlap of the two inner spherical shells S^1_I, S^2_I.

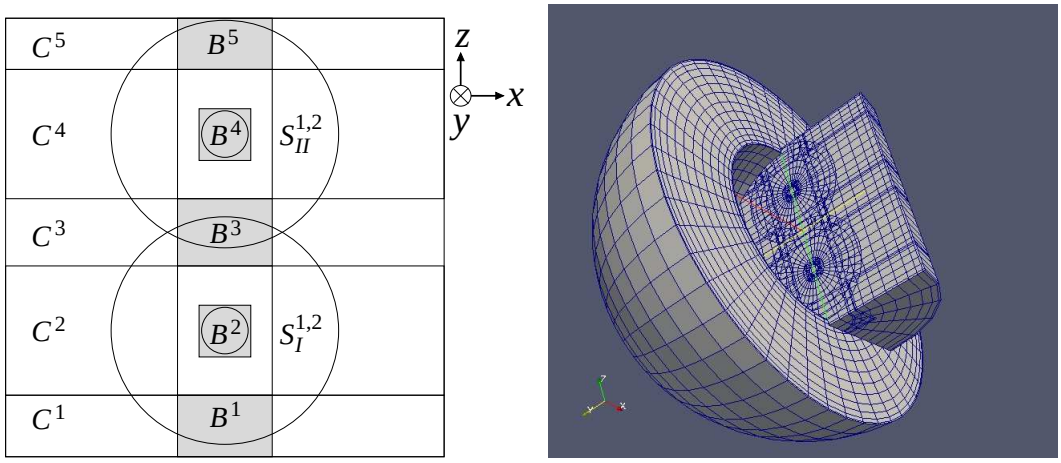

(a) inner domain decomposition (b) double cross section

FIGURE 3. 2-CENTER DOMAIN DECOMPOSITION FOR NEUTRON STAR PROBLEM. The left panel depicts the y-cross section of the inner subdomains with $S^1_{\rm out}$ suppressed. The right panel depicts all subdomains, although for the sake of visualization the outer radius for $S^1_{\rm out}$ has been chosen atypically small.

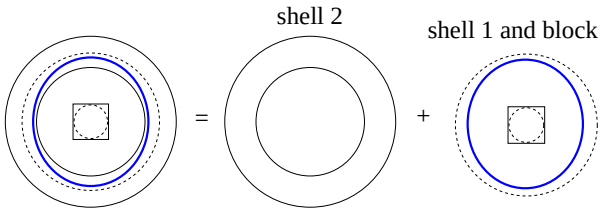

FIGURE 4. Subdomain configuration surrounding a stellar surface depicted as an elliptical bold curve.

3.2. **Modal-tau approximation of nonspherical stellar surfaces.** At each stellar surface regularity is lost both in the potential Φ and density ρ. Therefore, confinement of a stellar surface within a single spherical subdomain spoils spectral convergence. We describe a treatment of stellar surfaces which retains spectral convergence for $n = 0, 1, 2, 3, 4$.[3] Subsection 4.1 considers convergence for non-integer n. Our method also affords a low-rank treatment of the surfaces; see the text around Eqs. (23) and (24). The idea here is already evident in the model problem. As the "surface" $r = R$ changed in the model, the coefficient matrix approximating the Poisson operator only required a rank-2 update. Our low-rank treatment also pertains to the update of relevant preconditioners; see Subsection 3.3.

Consider the Poisson problem

$$\nabla^2\Phi = 4\pi G\rho(\mathbf{x}),\ \mathbf{x}\in D \quad \text{and} \quad \Phi(\mathbf{x}) = f(\mathbf{x}),\ \mathbf{x}\in\partial D, \tag{20}$$

where D is a 3d spherical ball with a 2d spherical boundary ∂D. For simplicity we have written down an isolated Dirichlet problem associated with D, but in practice D is a subregion of the BNS domain $\mathcal{D}$: either $B^2 \cup S^1_I \cup S^2_I$ or $B^4 \cup S^1_{II} \cup S^2_{II}$. Therefore, in practice interface conditions with the external subdomains (blocks and cylinders) would actually be specified on ∂D, i.e. the boundary values $f(\mathbf{x})$ are determined by the solution on these external subdomains. For concreteness and without loss of generality, let us assume D is the spherical region covered by $B^2 \cup S^1_I \cup S^2_I$. Then D contains one component closure(U_I) of the set closure(U), where the surface ∂U_I is nonspherical and a priori unknown. We view $B^2 \cup S^1_I$ as a single unit, the inner region of D. Likewise, we view S^2_I as the outer region of D. Shells S^1_I and S^2_I overlap, and by assumption this overlap contains the boundary component ∂U_I; see Fig. 3.2. We will continue with the example of star I and block 2. Therefore, for the rest of this subsection and the next one, we will suppress the I subscript and 2 superscript, writing simply $D = B \cup S^1 \cup S^2$.

Let $\widetilde{\Phi}^a_{\ell qn}$ represent the triply-indexed modal expansion coefficients on S^a for $a = 1, 2$. Here, the modal indices are $\ell = 0, \ldots, N_\theta$ dual to the polar angle, $q = 0, \cdots, N_\phi$ dual to the azimuthal angle, and $n = 0, \cdots, N^a_r$ dual to the radial coordinate. Throughout, S^1 and S^2 share the same angular resolution, so that N_θ and N_ϕ need not carry a superscript (subdomain index). We take $N_\phi = 2N_\theta$, although we enforce $\widetilde{\Phi}^a_{\ell qn} = 0$ for $q > 2\ell$. As described in [11], we keep the nonphysical coefficients $\{\widetilde{\Phi}^a_{\ell qn} : q > 2\ell\}$ to have the same data structure for the modal and nodal representations (convenient when using the spherical harmonic transform).

[3]However, for $n = 3, 4$ (which correspond to an unphysical neutron star EOS), one might expect numerical ill-conditioning due to shallow osculation of the density at stellar surfaces.

The representation of ∇^2 on a shell (either S^1 or S^2) is block-diagonal. Precisely, for each (ℓ, q) we have an (N_r+1)-by-(N_r+1) block. When $q > 2\ell$, each such block is the identity; however, the block corresponding to a physical mode $0 \le q \le 2\ell$ has the form [cf. Eq. (12)]

$$\left[\begin{array}{c} \mathbf{0} \\ \mathbf{0} \\ \hline \mathcal{BL}^{\ell q} \end{array}\right] = I_{r[2]} A_r^2 - 2B_{r[2]} A_r - \ell(\ell+1) B_{r[2]}^2. \tag{21}$$

Here $\mathbf{0}$ represents a row of zeros, and $\mathcal{BL}^{\ell q}$ is a sparse (N_r-1)-by-(N_r+1) submatrix (we use *superscripts* ℓ and q to label matrices). To address the issue of the coupling between the S^1 and S^2, first consider the case when C^1 continuity (in the solution) is imposed across a round sphere $r = R$, where the radial coordinate r is common to both spherical shells. Then the relevant submatrix $\mathcal{M}^{1:2,1:2} = \mathcal{M}^{1:2,1:2}(R)$ of the full coefficient matrix $\mathcal{M}$ (approximating the Laplacian over D) has the following structure [cf. Eq. (15)]:

$$\mathcal{M}^{1:2,1:2}(R) \equiv \left[\begin{array}{ccc|ccc} \ddots & & & & & \\ & \boxed{\begin{array}{c}\boldsymbol{\delta}^1(r^1_{\min}) \\ \boldsymbol{\delta}^1(R) \\ \mathcal{BL}^{1,\ell q}\end{array}} & & & \boxed{\begin{array}{c}\mathbf{0} \\ -\boldsymbol{\delta}^2(R) \\ \mathbf{0}\end{array}} & \\ \cdots & \vdots & \ddots & \cdots & \vdots & \cdots \\ \hline & \vdots & & \ddots & \vdots & \\ \cdots & \boxed{\begin{array}{c}-\boldsymbol{\nu}^1(R) \\ \mathbf{0} \\ \mathbf{0}\end{array}} & \cdots & \cdots & \boxed{\begin{array}{c}\boldsymbol{\nu}^2(R) \\ \boldsymbol{\delta}^2(r^2_{\max}) \\ \mathcal{BL}^{2,\ell q}\end{array}} & \cdots \\ & & & & & \ddots \end{array}\right], \tag{22}$$

here with generic (ℓ, q)-blocks (submatrices) of $\mathcal{M}^{1:2,1:2}(R)$ showcased. The tau conditions in the showcased off-diagonal blocks are responsible for the C^1 matching of the (ℓ, q)-mode across $r = R$. We stress that all other entries (indicated by horizontal dots) in these rows are zeros. However, when this C^1 matching is imposed across a nonspherical stellar surface described by a nontrivial envelope function $r = r(\boldsymbol{\theta})$, the showcased matching rows are replaced by full rows stretching across the whole of $\mathcal{M}^{1:2,1:2}$. More precisely, the following replacements are made in the above matrix:

$$\begin{aligned} [\cdots, \boldsymbol{\delta}^1(R), \cdots, \cdots, -\boldsymbol{\delta}^2(R), \cdots] &\to \boldsymbol{\beta}_{\ell q} \in \mathbb{R}^{1\times\mathcal{N}} \\ [\cdots, -\boldsymbol{\nu}^1(R), \cdots, \cdots, \boldsymbol{\nu}^2(R), \cdots] &\to \boldsymbol{\gamma}_{\ell q} \in \mathbb{R}^{1\times\mathcal{N}}, \end{aligned} \tag{23}$$

where

$$\mathcal{N} = [(N_r^1+1) + (N_r^2+1)](N_\theta+1)(2N_\theta+1) \tag{24}$$

is the number of rows (or columns) in the square matrix $\mathcal{M}^{1:2,1:2}$. Appendix C describes how these rows are filled; that is how the vectors $\boldsymbol{\beta}_{\ell q}$ and $\boldsymbol{\gamma}_{\ell q}$ are chosen. Since there are $(N_\theta+1)^2$ physical modes corresponding to each shell, the system sector corresponding to either shell 1 or 2 also has $(N_\theta+1)^2$ free rows of zeros in which to enforce matching conditions at the stellar surface; whence surface distortion corresponds to a rank-$2(N_\theta+1)^2$ update of $\mathcal{M}^{1:2,1:2}$.

Remark 3.1. *Representation of the Laplacian on the outer shell S^1_{out} also has the form* (21)*. Now, exterior solutions of the Poisson equation (with a compactly supported source)*

correspond to spherical harmonic modes of the form $r^{-(\ell+1)}Y_{\ell m}(\theta,\phi)$. *Therefore, for* $S^1_{\rm out}$ *we fill the second zero row of* (21) *with the tau-vector*

$$\boldsymbol{\nu}^1(r_{\rm out}) + r_{\rm out}^{-1}(\ell+1)\boldsymbol{\delta}^1(r_{\rm out}), \tag{25}$$

where $r_{\rm out}$, $\boldsymbol{\delta}^1(r_{\rm out})$, *and* $\boldsymbol{\nu}^1(r_{\rm out})$ *are respectively the outer radius, a Dirichlet vector, and a Neumann vector belonging to* $S^1_{\rm out}$. *These tau-conditions define the nonlocal boundary condition* $\mathcal{B}(\Phi)=0$ *in* (19).

3.3. **Preconditioning.** Solution of the problem (20) on the subregion $D = B\cup S^1\cup S^2 \subset \mathcal{D}$ is one ingredient of the preconditioner for solving the 2-center Poisson problem on $\mathcal{D}$. Both the $\mathcal{D}$- and D-problems are solved by preconditioned GMRES; here we discuss the preconditioner for the D-problem (in a sense the preconditioner of the preconditioner). The relevant preconditioner is a block-Jacobi preconditioner which features, in part, inversion of the block-diagonal part $\mathcal{G}$ of $\mathcal{M}^{1:2,1:2}$. That is, $\mathcal{G}$ is comprised of the $(N_\theta+1)^2$ diagonal blocks of $\mathcal{M}^{1:2,1:2}$ which correspond to physical (ℓ,q)-modes, in addition to identity-matrix blocks associated with the non-physical modes ($q>2\ell$). Since the diagonal blocks of $\mathcal{G}$ are themselves sparse, we should perhaps take advantage of this fact in applying $\mathcal{G}^{-1}$. However, thus far we have simply computed and used the LU-factorizations of each physical-mode block. Now, if we view $N\sim N_r^1\sim N_r^2\sim N_\theta$, then the total number of physical modes belonging to shell 1 and 2 is $(N_r^1+N_r^2+2)(N_\theta+1)^2\sim 2N^3\sim\frac{1}{2}\mathcal{N}$, where $\mathcal{N}$ is the total number of modes (24). With this perspective, the LU-factorization of all nontrivial blocks comprising $\mathcal{G}$ costs $O\big((N_\theta+1)^2[(N_r^1+1)^3+(N_r^2+1)^3]\big)=O(\mathcal{N}^{5/3})$ work. Likewise, with these precomputed LU-factorizations, application of $\mathcal{G}^{-1}$ costs $O\big((N_\theta+1)^2[(N_r^1+1)^2+(N_r^2+1)^2]\big)=O(\mathcal{N}^{4/3})$ work.

While $\mathcal{G}^{-1}$ serves as an excellent preconditioner when the stellar surface is spherical, its effectiveness deteriorates as the surface distorts. We therefore consider correction based on the Sherman-Morrison-Woodbury formula. Suppose now that $\mathcal{M}^{1:2,1:2}$ is (22) with the replacements (23). We may then write

$$\mathcal{M}^{1:2,1:2} = \mathcal{G}+\mathcal{U}\mathcal{V}, \tag{26}$$

with the matrix $\mathcal{V}\in\mathbb{R}^{2(N_\theta+1)^2\times\mathcal{N}}$ built from the non-zero rows of $\mathcal{M}^{1:2,1:2}-\mathcal{G}$ and $\mathcal{U}\in\mathbb{R}^{\mathcal{N}\times 2(N_\theta+1)^2}$ a matrix of zeros, apart from a single 1 appearing in some if its rows. By the Sherman-Morrison-Woodbury formula

$$(\mathcal{G}+\mathcal{U}\mathcal{V})^{-1} = [I-\mathcal{G}^{-1}\mathcal{U}\mathcal{C}^{-1}\mathcal{V}]\mathcal{G}^{-1}, \qquad \mathcal{C}\equiv I+\mathcal{V}\mathcal{G}^{-1}\mathcal{U}. \tag{27}$$

Here $\mathcal{C}$ is the *capacitance matrix*. The main cost in applying the inverse of $\mathcal{M}^{1:2,1:2}$ is then the cost of inverting the capacitance matrix, here assuming a direct inversion. Subject to the assumptions just made, this cost is $O\big([2(N_\theta+1)^2]^3\big)=O(N^6)=O(\mathcal{N}^2)$. While this cost might be reduced further via a different strategy for inversion of $\mathcal{C}$, the chief walltime cost (currently and empirically) stems from the computation of $\mathcal{V}$; see Appendix C.

3.4. **Solution procedure for co-moving binaries.** Given in **Algorithm 2**, our procedure for construction of co-moving Newtonian binaries mirrors the procedure outlined for single stars. We use the SCF method [46] of Ostriker and Mark with regularizations of a type first consider by Hachisu [5]. The next two paragraphs address the need for regularization.

Assuming a fixed EOS and gravitational constant G, a Newtonian binary pair is determined by three physical fixations: the stellar masses M_I, M_{II} and the separation d. In addition, five extra gauge fixations are required to locate the pair in $\mathbb{R}^3$. Fixation of d and

the five gauge choices is equivalent to fixation of each star's center-of-mass, here assuming Cartesian coordinates which co-rotate with the binary. For the centers-of-mass we effectively choose $(0, 0, C_{z,I})$ and $(0, 0, C_{z,II})$, with $C_{y,I} = 0 = C_{y,II}$ and $C_{x,I} = 0 = C_{x,II}$ respectively enforced by the reflection symmetries across the $y = 0$ and $x = 0$ planes. Therefore, we might view a Newtonian binary as determined by four fixations: M_I, M_{II}, $C_{z,I}$, $C_{z,II}$.

To ensure convergence to a unique solution (*regularize* the associated fixed-point iteration), an SCF method for binaries must deal with the physical and gauge issues raised in the last paragraph. The fixations of M_I, M_{II}, $C_{z,I}$, and $C_{z,II}$ are integral conditions involving the stellar density. While we have used these integral conditions [49], here we adopt regularization approaches based on easier-to-implement pointwise conditions. These pointwise conditions stem from (19b) itself, and they define κ_I, κ_{II}, Ω^2, ℓ_z. We refer to one regularization approach as HACHISU [5, 6, 7], and the other as MEUDON [27]. For example, the MEUDON approach amounts to fixation of $\rho_{\max,I}$, $\rho_{\max,II}$, $\mathbf{x}_I = (0, 0, z_I)$, $\mathbf{x}_{II} = (0, 0, z_{II})$, again with $\mathbf{x}_{I,II}$ the maxima locations. The choice of regularization approach affects lines 3 and 6 in **Algorithm 2**. This subsection describes each line of **Algorithm 2**. We often deal only with star I, with the understanding that our descriptions also pertain to star II.

Algorithm 2 BINARY SCF ITERATION. Inputs are (i) modal coefficients for the enthalpy $h(\mathbf{x})$ on B^2 and S^1_I; (ii) modal coefficients for $h(\mathbf{x})$ on B^4 and S^1_{II}; (iii) the scalars $\kappa_{I,II}$, Ω^2, ℓ_z; and (iv) a preconditioner for the Poisson solve. Outputs are updates of the same objects.

1: Find the zero sets (stellar surfaces) $r_{I,II}(\boldsymbol{\theta}_{I,II})$ of the enthalpy $h(\mathbf{x})$.
2: By **Algorithm 3** compute matrices $\widetilde{E}^{I,II}_{1,1:2}$ and $\widetilde{F}^{I,II}_{2,1:2}$ determining matching conditions.
3: Obtain new density $\rho(\mathbf{x})$ from $h(\mathbf{x})$ as modal coefficients on the subdomains $B^{2,4}$, $S^1_{I,II}$.
4: Update the preconditioner for the Poisson solve.
5: Solve the (numerical approximation to the) problem $\nabla^2\Phi = 4\pi G\rho(\mathbf{x})$, $\mathcal{B}(\Phi) = 0$.
6: Get updated scalars $\kappa_{I,II}$, Ω^2, ℓ_z.
7: Update enthalpy via the generalized potential equation.
8: Enforce symmetries on the enthalpy.

3.4.1. *Surface location and update of matching conditions (lines 1 and 2).* For each angular direction $\boldsymbol{\theta}_{jk}$ on shell S^1 the modal coefficients $\widetilde{h}^1_{\ell qn}$ of the enthalpy define a radial function

$$\mathcal{P}_{N^1_r,N_\theta} h(r\boldsymbol{\theta}_{jk}) = \sum_{\ell=0}^{N_\theta} \sum_{q=0}^{2N_\theta} \sum_{n=0}^{N^1_r} \widetilde{h}^1_{\ell qn} \mathcal{E}^1_{\ell qn}(r, \theta_j, \phi_k), \tag{28}$$

where the basis functions $\mathcal{E}^1_{\ell qn}(r, \theta_j, \phi_k)$ appear in (53). Using the bisection method, we find the root r_{jk} of $\mathcal{P}_{N^1_r,N_\theta} h(r\boldsymbol{\theta}_{jk})$, typically with a tolerance near machine precision. Via the discrete spherical harmonic transform, the grid function r_{jk} may be converted to the coefficients $\widetilde{r}_{\ell q}$ of its corresponding spherical harmonic expansion. For line 2 the tau-vectors introduced abstractly in (23) are given by

$$\begin{aligned} \boldsymbol{\beta}_{\ell q} &= \widetilde{E}_{1,1:2}(\ell(2N_\theta + 1) + q, :) \\ \boldsymbol{\gamma}_{\ell q} &= \widetilde{F}_{2,1:2}(\ell(2N_\theta + 1) + q, :), \end{aligned} \tag{29}$$

where Appendix C describes precisely how to compute the matrices $\widetilde{E}_{1,1:2}$ and $\widetilde{F}_{2,1:2}$. These matrices define the low-rank update described near the end of Subsection 3.2.

3.4.2. *Obtainment of density from enthalpy (line 3).* Let $\widetilde{h}^B_{ijk}$ and $\widetilde{h}^1_{\ell qn}$ denote the modal coefficients for the enthalpy on the subdomains B^2 and S^1_I. From these coefficients the goal is to obtain modal coefficients $\widetilde{\rho}^B_{ijk}$ and $\widetilde{\rho}^1_{\ell qn}$ for the density via the EOS. The HACHISU and MEUDON approaches achieve this goal differently, although for both $\rho_{\max,I}$ remains fixed throughout the algorithm (even outside of line 3).

- The HACHISU approach begins with a search for the maximum value $h_{\max,I}$ of the enthalpy and the point $\mathbf{x}_I = (0, 0, z_I)$ where it occurs; here, we assume $\mathbf{x}_I \in B^2$. Note that $h_{\max,I}$ and $\mathbf{x}_I$ change when the enthalpy does (in line 7).
- The MEUDON approach involves no search, and both $h_{\max,I} \equiv K_I(n+1)\rho^{1/n}_{\max,I}$ and $\mathbf{x}_I$ remain fixed (even outside of line 3). We have not tried the MEUDON approach for $n = 0$.

With $h_{\max,I}$ in hand (whether computed through a search, or fixed throughout), we are ready to compute the density. First, define the ratio $C = \rho_{\max,I}/h^n_{\max,I}$ which is $[K_I(n+1)]^{-n}$ for the MEUDON case. Next, based on the polytropic index n, proceed as follows.

- For $n = 1$ set $\widetilde{\rho}^B_{ijk} = C\widetilde{h}^B_{ijk}$ and $\widetilde{\rho}^1_{\ell qn} = C\widetilde{h}^1_{\ell qn}$ for all indices.
- For $n \neq 1$ first use the inverse spectral transforms associated with B^2 and S^1_I (respectively, a triple-Chebyshev transform and a Chebyshev-spherical-harmonic transform) to compute collocation values for the enthalpy. On B^2 these collocation values are assumed positive; therefore, restrict attention to the collocation values $h^1_{\ell qn}$ on S^1_I. Some values $h^1_{\ell qn}$ will be positive, and others negative. Provided $h^1_{\ell qn} \geq 0$, the corresponding density value is simply $\rho^1_{\ell qn} = C(h^1_{\ell qn})^n$. Now consider the case $h^1_{\ell qn} < 0$.
  - For $n = 0, 2, 3, 4$ we again set $\rho^1_{\ell qn} = C(h^1_{\ell qn})^n$.
  - For n not integer, we may set $\rho^1_{\ell qn} = \pm C|h^1_{\ell qn}|^n$ or 0. In practice, these choices all yield similar performance.

  Once all collocation values (on both B^2 and S^1_I) for the density have been computed, we obtain the corresponding modal coefficients via the spectral transforms.

Regardless of n, the described steps yield the modal coefficients for the density on B^2 and S^1_I. However, unless n is an integer, the modal coefficents $\widetilde{\rho}^1_{\ell qn}$ will not exhibit rapid decay.

Remark 3.2. *The support of the true physical density ρ defines the stellar extents, as discussed in the first paragraph of Section 3. Whence by definition the physical ρ vanishes on the region exterior to both stars. Nonetheless, a feature of our numerical method is the double-valuedness of ρ's numerical representation on the overlap $S^1_I \bigcup S^2_I$ which contains the current stellar surface at each SCF step. On S^1_I and exterior to the current surface, ρ's numerical representation may be nonzero, as seen in the prescription just given. Therefore, on the overlap and exterior to the surface, our approximation to the physical density must be ρ's numerical representation on S^2_I which always vanishes.*

3.4.3. *Preconditioner update and Poisson solve (lines 4 and 5).* With the new stellar surface, the preconditioner is updated via the Sherman-Morrison-Woodbury identity as described in Subsection 3.3. Reference [11] presents most of the details for the global Poisson solve listed in line 5. The solve in line 5 incorporates the new surface matching conditions from line 2.

3.4.4. *Parameter update (line 6).* The MEUDON approach corresponds to the choice of equations in (19c). These determine that the enthalpy (and so also the density) attains prescribed maximum values at the points $\mathbf{x}_{I,II}$. Owing to enforcement of symmetry assumptions, only

z-partial derivatives are necessary in the formulation of these conditions. Combination of (19b,c) yields the following system of equations:

$$\kappa_I = K_I(n+1)\rho_{\max,I}^{1/n} + \Phi(\mathbf{x}_I) - \tfrac{1}{2}(z_I - \ell_z)^2\Omega^2 \tag{30a}$$

$$\kappa_{II} = K_{II}(n+1)\rho_{\max,II}^{1/n} + \Phi(\mathbf{x}_{II}) - \tfrac{1}{2}(z_{II} - \ell_z)^2\Omega^2 \tag{30b}$$

$$0 = \frac{\partial\Phi}{\partial z}\Big|_{\mathbf{x}=\mathbf{x}_I} - (z_I - \ell_z)\Omega^2 \tag{30c}$$

$$0 = \frac{\partial\Phi}{\partial z}\Big|_{\mathbf{x}=\mathbf{x}_{II}} - (z_{II} - \ell_z)\Omega^2. \tag{30d}$$

Here the terms involving the gravitational potential are viewed as known; they are computed with the solution to the Poisson problem in line 5. Equations (30) are then viewed as a nonlinear system for the parameters $\kappa_I, \kappa_{II}, \Omega^2, \ell_z$, and we solve it via Newton's method.

For the simplifying case of an equal-mass binary, the HACHISU approach assumes that the surface of star I, say, intersects the z-axis at prescribed points, here taken as z_A and z_B. Then the system which determines the parameters is

$$\kappa_I = \Phi(\mathbf{x}_A) - \tfrac{1}{2}z_A^2\Omega^2 \tag{31a}$$

$$\kappa_I = \Phi(\mathbf{x}_B) - \tfrac{1}{2}z_B^2\Omega^2. \tag{31b}$$

Again with the gravitational potential terms considered as known data, the system in (31) is solved for κ_I and Ω^2, along with the conditions $\kappa_{II} = \kappa_I$ and $\ell_z = 0$. A more complicated system is necessary for the unequal-mass scenario. We consider the generic version of the HACHISU approach in Appendix D.

3.4.5. *Enthaply update (lines 7 and 8).* For line 7 use of the solved-for parameters (described in the last two paragraphs) ensures that, when it is computed from (19b) and the solution Φ obtained in line 5, the new enthalpy respects the required constraints (19c), or similar constraints defined in the HACHISU approach. The enthalpy configuration for a Newtonian binary is symmetric with respect to reflection across both the $x = 0$ or $y = 0$ planes. We perform line 8 by setting to zero (by hand) certain modes on B^2, B^4,S_I^1, and S_{II}^1.

4. NUMERICAL RESULTS FOR BINARIES

This section presents the results of our 3d numerical experiments. Its first subsection considers a single 3d Poisson solve involving a binary star density distribution with mock nonspherical surfaces $\partial U_{I,II}$. Next, using regularized versions of the SCF method, its second subsection considers construction of binaries. Throughout, this section uses the BNS domain $\mathcal{D}$ specified in Table 1, or an overall scaling of it. To document convergence, we associate with $\mathcal{D}$ a sequence of resolutions listed in Table 2. In the table and throughout this Section 4, we assume Chebyshev indexing from 1; whence, for example, now $N_x^{B^1} = 14$ means 14 modes not 15. $N_\phi^{C^1} = 5$ means 5 Fourier modes. As before, $\ell_{\max}^{S^1_{\text{out}}} = 10$ means 121 spherical harmonic modes. Our GMRES tolerance choices (stopping criteria on the relative residual) for the sequence levels have been `1.0e-09`, `1.0e-10`, `1.0e-11`, and `9.0e-12`. These tolerances are overly stringent. Nevertheless, for our multilevel preconditioner (see [11]) we have chosen tolerances which are 10 times smaller for the GMRES solves associated with subregions of $\mathcal{D}$. For all documented experiments, we have performed 3 sweeps of the additive Schwarz preconditioner described in [11].

Spherical shells				
S^1_I: $0.01 \le r \le r_{\max,I}$;	S^2_I: $r_{\min,I} \le r \le 1.0$;	S^1_{II}: $0.01 \le r \le r_{\max,II}$;	S^2_{II}: $r_{\min,II} \le r \le 1.0$;	S^1_{out}: $2.04 \le r \le 10.0$
Cylindrical shells (all with $r_{\max,I} + 0.01 \le \rho \le 2.24$ and $0 \le \phi \le 2\pi$)				
C^1: $-2.24 \le z \le -1.57$;	C^2: $-1.57 \le z \le -0.43$;	C^3: $-0.43 \le z \le 0.43$;	C^4: $0.43 \le z \le 1.57$;	C^5: $1.57 \le z \le 2.24$
Blocks (B^2, B^4 with $-0.0105 \le x, y \le 0.0105$; B^1, B^2, B^3 with $-0.57 \le x, y \le 0.57$)				
B^1: $-2.24 \le z \le -1.57$;	B^2: $-1.0105 \le z \le -0.9895$;	B^3: $-0.43 \le z \le 0.43$;	B^4: $0.9895 \le z \le 1.0105$;	B^5: $1.57 \le z \le 2.24$

TABLE 1. 2-CENTER BNS DOMAIN. The center of B^2, S^1_I, and S^2_I is $(0, 0, z_I)$ with $z_I = -1.0$. The center of B^4, S^1_{II}, and S^2_{II} is $(0, 0, z_{II})$ with $z_{II} = 1.0$. We set $r_{\max,I} = 1.1R_I$, $r_{\min,I} = 0.9R_I$, $r_{\max,II} = 1.1R_{II}$, $r_{\min,II} = 0.9R_{II}$, and subsequently chopped each of these values to two digits. $R_{I,II}$ values are given below.

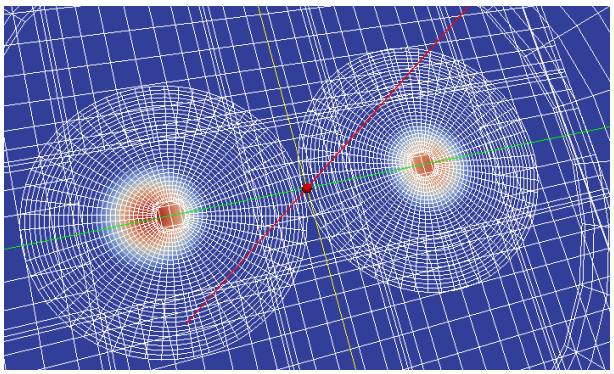

FIGURE 5. DENSITIES FOR TWO LANE-EMDEN STARS. The center of each star has been placed off-center relative to the nearest coordinate center in the 2-center global domain. Here this off-centering is exaggerated.

4.1. **Poisson problem on 2-center domain.**

4.1.1. *Polytropic index* $n = 1$. We consider the exact solution corresponding to the superposition of two Newtonian Lane-Emden stars. Each star separately obeys $\nabla^2\Phi = 4\pi G\rho$, with $G = 1$ and the solution given by $\rho(\eta)$ and $\Phi(\eta)$ from (3) in terms of the radial distance η from the stellar center. Here we have used η rather than r, since the latter will denote the radial coordinate within a spherical shell. We use the formulas in (3) to fix pairs $\{\Phi_I, \rho_I\}$ and $\{\Phi_{II}, \rho_{II}\}$, one for each of the centers. We choose $\rho_{c,I} = 1.0, R_I = 0.40625$ and $\rho_{c,II} = 1.0, R_{II} = 0.40625$. Superposition $\Phi = \Phi_I + \Phi_{II}$ of the two potentials yields an exact solution to the Poisson problem corresponding to the superposed non-overlapping densities.

We will numerically solve for Φ and compare the result with the exact solution. To make the problem more challenging and reflective of the situation encountered with gravitationally interacting stars, we do not choose the centers of the stars to coincide with the centers of the global 2-center domain. Instead, we place the stellar centers at $(0, 0, z_I)+\Delta\boldsymbol{x}_I$ and $(0, 0, z_{II})+\Delta\boldsymbol{x}_{II}$ For the experiment documented here, $\Delta\boldsymbol{x}_I$ = `(+2.64e-3,-1.01e-2,2.46e-2)` and $\Delta\boldsymbol{x}_{II}$ = `(-8.14e-3,+2.22e-3,-2.60e-2)`. With these choices for $\Delta\boldsymbol{x}_I, \Delta\boldsymbol{x}_{II}$, each stellar surfaces is contained in the overlap between the relevant two inner spherical shells. The qualitative nature of the resulting Lane-Emden densities ρ_I, ρ_{II} is depicted in Fig. 5. As a result, with respect to the spherical polar coordinates on the inner spherical shells, each stellar surface is a mock nonspherical surface, i.e. not a fixed coordinate radius locus. For

	$N_x^{B^1}$	$N_y^{B^1}$	$N_z^{B^1}$	$N_x^{B^2}$	$N_y^{B^2}$	$N_z^{B^2}$	$N_r^{S_I^1}$	$\ell_{\max}^{S_I^1}$	$N_r^{S_I^2}$	$N_r^{C^1}$	$N_\phi^{C^1}$	$N_z^{C^1}$	$N_z^{C^2}$	$N_r^{S_{\text{out}}^1}$	$\ell_{\max}^{S_{\text{out}}^1}$
Level 1	14	14	7	7	7	7	12	12	12	13	5	7	17	25	10
Level 2	19	19	9	9	9	9	15	16	15	19	9	9	23	85	18
Level 3	24	24	11	11	11	11	18	20	18	23	13	11	29	105	24
Level 4	27	27	15	15	15	15	22	24	22	26	15	15	32	117	30

TABLE 2. TRUNCATIONS FOR THE POISSON SOLVE EXPERIMENT. Each table row lists enough information to recover the truncations used on each subdomain of $\mathcal{D}$. The truncations for blocks B^3 and B^5 are the same as those for B^1; the truncations for block B^4 are the same as those for B^2; $\ell_{\max}^{S_I^2} = \ell_{\max}^{S_I^1}$; truncations for star *II* are the same as for star *I*; all cylinders have the same radial and azimuthal truncations, with $N_z^{Cj} = N_z^{C1}$ for $j = 3, 5$ and $N_z^{C4} = N_z^{C2}$.

	MPSPD	L_2 err	L_2 norm	L_∞ err	L_∞ norm	iters	tol
Level 1	10.92	6.9464e-07	2.3520e-01	7.9417e-06	4.6382e-01	10	1.0000e-09
Level 2	16.85	8.5983e-08	1.7796e-01	4.4325e-07	4.6412e-01	7	1.0000e-10
Level 3	21.36	2.1830e-09	1.7009e-01	2.1837e-08	4.6400e-01	6	1.0000e-11
Level 4	25.53	6.8931e-12	1.7378e-01	1.5055e-10	4.6412e-01	4	9.0000e-12

TABLE 3. ERRORS AND NORMS CORRESPONDING TO THE TRUNCATIONS IN TABLE 2. Listed quantities have been computed after suitable inverse transformations on each subdomain to yield nodal values. The L_∞ norms do not settle down quickly as the spectral grids associated with nodal values are relatively coarse.

each angular direction we find the radial value of the surface via Newton's method. Upon using the spherical harmonic transform, we then obtain a spherical harmonic expansion for each surface (the expansion could be found analytically as well).

Our first test is to solve the $n = 1$ Poisson problem for the above sequence of truncations. Table 3 lists the errors corresponding to the levels in Table 2. A numerical solution is a collection of modal expansion coefficients; however, comparisons with the exact solution are always computed in physical space on the nodal grid (or grids in this multidomain case) dual to the modal expansion. These nodal grids are coarse, and the norms reported in Table 3 do not settle down quickly. To address the issue of whether or not the convergence apparent in Table 3 is "spectral", we have also included the column MPSPD or *modes per subdomain per dimension*. This number gives a rough indication of the resolution, and the error decays exponentially fast as it increases.

4.1.2. *Polytropic index* $n \neq 1$. We now consider the experiment just described, only now with $n = \frac{1}{2}$ and $\frac{3}{2}$. Appendix B describes how we generate sufficiently accurate one-dimensional reference solutions to the Lane-Emden ODE when an exact solution is not available. Such solutions are used to compute the errors reported in Fig. 6. For non-integer n the density exhibits one-sided loss of regularity as the stellar surface is approached from the inside. As a result, the spectral convergence documented above for $n = 1$ breaks down. We therefore stop

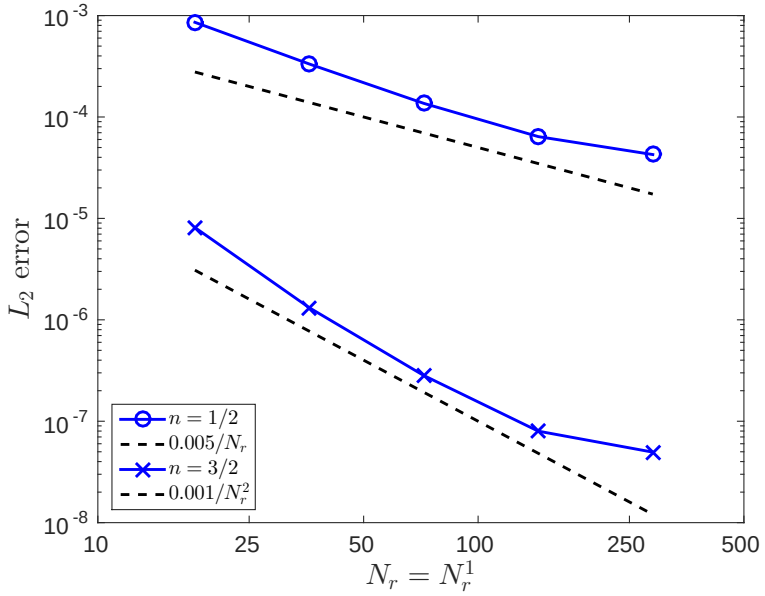

FIGURE 6. LANE-EMDEN SOLUTION WITH FRACTIONAL n. Here we consider same experiment with Level 3 and $n = 1/2, 3/2$.

the sequence of resolutions at Level 3, subsequently increasing the radial resolution in the shells S_I^1 and S_{II}^1. One might think of these partially increased resolutions as Level 3b, Level 3c, etc. Now, Level 3 (or Level 3a) has $N_r = N_r^{S_I^1} = N_r^{S_{II}^1} = 18$, Level 3b has $N_r = 36$, and we continue to Level 3e with $N_r = 288$. Figure 6 documents the convergence, in comparison with linear ($\propto 1/N_r$) and quadratic ($\propto 1/N_r^2$) trends. For both $n = \frac{1}{2}$ and $\frac{3}{2}$ cases the slow down in convergence seen near $N_r = 288$ can be ameliorated through increased angular resolution in both of the shells surrounding the surface. For a nodal method, Ref. [47] has described a method for alleviating the slow-down in convergence for "stiff equations of state" ($0 < n < 1$). While we believe the strategy presented in that reference can be adapted to our approach, we have yet to implement it.

4.2. **Binary problems.** Using the SCF method described above, this subsection constructs Newtonian co-moving binaries. Since exact solutions are not available for such configurations, in addition to the levels in Table 2, we consider another reference level, essentially `Level 5`, obtained from `Level 4` by adding 1 to all truncations, save for the resettings $N_r^{S_{\rm out}^1} = 120$ and $\ell_{\rm max}^{S_{\rm out}^1} = 32$. The GMRES tolerance `4.0e-12` has been chosen for this fifth level.

4.2.1. *Convergence study for $n = 1$ case.* This subsection documents a self-convergence study for an unequal mass configuration. For `Level 1` through `Level 5` (the reference level) we have chosen $30, 20, 20, 10, 10$ for the number of SCF iterations. Moreover, the output solution (enthaply) for each level has served as the initial guess for the SCF iteration at the next level. Therefore, only `Level 1` requires a starting configuration, and for it we have superposed two spherically symmetric $n = 1$ Lane-Emden stars with $\rho_{c,I} = 0.5, R_I = 0.375$ and $\rho_{c,II} = 1.0, R_{II} = 0.411432604093155$. As described in Appendix B, these choices determine both the constant $K_{I,II}$ in the EOS and the masses $M_{I,II}$. Since we know the coordinate distance between the star's centers, we then use Kepler's law to fix the initial Ω^2.

	truncation	shell error	cube error	surface error	virial check
Level 1	29752	4.4393e-06	6.0939e-06	1.2841e-06	1.0515e-06
Level 2	117103	9.0547e-07	9.5293e-07	5.3233e-08	2.1960e-07
Level 3	239496	2.8059e-08	3.0330e-08	3.8459e-10	6.5556e-09
Level 4	411112	1.0389e-10	9.6746e-11	9.7438e-12	1.6059e-11
REFERENCE	474464	---	---	---	5.0718e-12

TABLE 4. CONVERGENCE STUDY ERRORS. Here we list errors measured against the reference solution for the unequal mass convergence study. These errors correspond to the truncations in Table 2, and the main text describes how they have been computed. The `REFERENCE` (essentially `Level 5`) results from slight increase of the truncations for `Level 4`; see the text.

Table 4 list results. The truncation column lists the number of unknowns, including unphysical spherical harmonic modes; see the text before (21). For example, the number of physical modes for `Level 4` is only 249502, corresponding to the reported 25.53 MPSPD. All listed errors are relative 2-norm errors measured against the reference configuration. More precisely, for the "cube error" and "shell error" we have, for each level, interpolated the numerical solution for the gravitational potential Φ onto two fixed uniform grids: one associated with B^4 ($N_x^0 = N_y^0 = N_z^0 = 11$) and the other with $S^1_{\rm out}$ ($N_r^0 = 21$, $N_\theta^0 = 41$, $N_\phi^0 = 41$). The "surface error" listing also arises as the relative 2-norm errors against the reference grid. Here, for each level, the numerical solution for the surface $r_{II}(\boldsymbol{\theta}_{II})$ has been interpolated onto a fixed uniform grid ($N_\theta^0 = 41$, $N_\phi^0 = 41$). The viral check [5, 48] constitutes an independent check on the errors. The expression we have evaluated is

$$\text{V.C.} \;= |2T + W + 3P| \big/ |W|, \tag{32}$$

where the rotational energy T, gravitational energy W, and pressure volume integral P are

$$\begin{aligned} W &= \Big[\int_{\text{star } I} + \int_{\text{star } II} \Big] d\mathbf{x} \tfrac{1}{2} \rho(x) \Phi(\mathbf{x}) \\ T &= \Big[\int_{\text{star } I} + \int_{\text{star } II} \Big] d\mathbf{x} \tfrac{1}{2} \rho(x) \Omega^2 \varpi^2(\mathbf{x}) \\ P &= \Big[\int_{\text{star } I} + \int_{\text{star } II} \Big] d\mathbf{x} (n+1)^{-1} h(\mathbf{x}) \rho(\mathbf{x}). \end{aligned} \tag{33}$$

Numerical evaluation of these integrals is discussed in Appendix E. The virial check along with the other listings in Table 4 suggest that the reference solution is accurate to about 11 digits. Furthermore, the table indicates spectral convergence; the results therein validate our approach and its implementation.

4.2.2. *Comparison with Hachisu results.* This subsection demonstrates that our results agree with much earlier results [6] of Hachisu for an equal-mass case. We adopt the described HACHISU approach to regularized the SCF iteration, including the parameter conditions (31). Moreover, in line 8 of Algorithm 2, we enforce symmetries across all three coordinate planes. Throughout, our discussion makes use of the same 2-center domain $\mathcal{D}$ and levels (truncation choices) described earlier.

	$-z_B$	Ω^2	$P_{\max}$	virial check
Level 2	0.333	0.1124772008204 (0.112)	0.2059169485482 (0.207)	1.4337e-07
Level 3		0.1124770770717	0.2059169765393	9.4858e-10
Level 4		0.1124770783021	0.2059169766070	5.9824e-12
Level 4	0.417	0.0669516423484 (0.0695)	0.1661144339967 (0.166)	2.4793e-11
Level 4	0.500	0.0370452955356 (0.0387)	0.1261597690337 (0.128)	9.7199e-11

TABLE 5. COMPARISON TO HACHISU'S RESULTS IN [6]. The table entries correspond to an equal-mass $n = 0$ configuration, and the negative values of r_B (our z_B) listed in TABLE 1, page 466 of that reference. Numbers within parenthesis are Hachisu's values. In view of the virial-check errors, in some cases (for the sake of consistency in the format) we have listed more digits than are trustworthy.

We consider $n = 0$, resulting in a discontinuous stellar surface. To facilitate the comparison, we choose both $R = R_I = R_{II}$ and scale the domain $\mathcal{D}$ in Table 1 in order to ensure that the star-I extents obey the following along the z-axis: $-1 = z_A \leq z \leq z_B = -(1-R)/(1+R)$. Due to the auxiliary equations (31) enforced in the HACHISU prescription, the z-extents of the stars remain fixed throughout the SCF iteration. Table 5 collects our results for several choices of z_B considered in [6]. Values listed in parenthesis come from [6]. More precisely, they stem from "TABLE 1, POLYTROPES (two-body system)", page 466 of that reference, where they are associated with *negative* r_B. The minus sign is Hachisu's notation to distinguish detached binaries from disk-shaped structures; his r_B is our z_B which is negative since star I lies on the negative z-axis. As in [6], we have listed only 3 digits for z_B, but our table choices have been determined by the following R values: $\frac{1}{2}$, 0.411432604093155, and $\frac{1}{3}$. In all cases $\rho_{\max,I} = 1 = \rho_{\max,II}$.

Hachisu lists values for Ω^2, M (mass), V (volume), J (angular momentum), T, $-W$, 3Π (our $3P$ above), and $P_{\max}$ (maximum pointwise pressure). Since we have found similar agreement in all of these quantities, Table 5 only collects values for Ω^2 and $P_{\max}$. As indicated in the table, for $z_B = -0.333$ we again consider several levels, increasing the truncation to document convergence. Based on the virial check, Hachisu claimed values good to about 3-digit accuracy. Our results confirm this assertion.

5. CONCLUSIONS

We conclude with criticism of the present work and a summary of future work towards construction of helically symmetric spacetimes.

We have presented a new spectral method for the treatment of stellar surfaces in binary neutron star models. While the method has been tested only for co-moving Newtonian binaries, in principle it is applicable to both counter-rotational Newtonian binaries and relativistic binaries, say solution of the conformal thin-sandwich equations describing quasi-equilibrium binary initial data. We have described the method as low-rank, since stellar surfaces are reflected through tau-conditions in the bulk operator.

The low-rank description implies that our approach is more efficient than a nodal one based on surface-adapted coordinate transformations. However, despite this intimation, the reality of such an assertion has not been put to the test here. Ideally, we would compare

our approach to either (or both) of the ones implemented in the LORENE or SpEC codes. The details involved in the nodal approach (for example, the type of preconditioning) are notably different. While such a comparison would be of interest, it would also be a significant undertaking. Moreover, such comparison would ideally be made beyond the relatively simple co-moving Newtonian scenario, as is possible with both LORENE or SpEC (we are currently working to move beyond this scenario). We do note that some comparison of our modal approach toward preconditioning with traditional nodal strategies appears in [12]. As a final criticism, we note that our work has not made extensive use of parallelism. While for many fields (see below) we have exploited parallelism, we should parallelize the application of our preconditioner, with tasks determined by the subdomains or even the particular modes on each subdomain. While we believe this issue holds promise, as the sole code developer the author of this work has not yet been able to pursue it.

The next step in our goal of numerically constructing helically symmetric spaces is to replace the Laplacian in the Newtonian problem with the helically reduced wave operator, that is to move from the Poisson problem to the HRWE. This step is taken in the proceedings [49]. They key technical challenges are (i) inclusion of the angular momentum term in the bulk operator and (ii) in the HRWE-based problem the only symmetry corresponds to reflection about the orbital plane $y = 0$. The challenge presented by (i) is formidable, but we have already met it in [11]. With regard to (ii), our approach has been to introduce another parameter (ℓ_x, always zero in this work). Moreover, rather than the pointwise conditions adopted here to regularize the SCF algorithm, [49] has adopted integral regularization conditions. Proper treatment of issue (ii) proves crucial in achieving numerical convergence for the generalized SCF method.

On a different tack, future work will also describe use of the Broyden algorithm [50] to accelerate the SCF method which is essentially a fixed-point iteration. Work [51] in progress focuses on BNS approximations inspired by the post-Minkowski formalism. We hope that this effort will result in (trial data for) binary initial data largely uncontaminated by junk radiation. After these steps, we might consider our ultimate goal of solving the helically reduced Einstein equations.

6. ACKNOWLEDGMENTS

I wish to thank Richard Price for bountiful correspondence and discussions on the work presented here. I am also grateful for helpful comments from Daniel Appelö, Tom Hagstrom, Monika Nitsche, Deborah Sulsky, and an anonymous referee. This work has been supported through NSF grant No. DMS 1216866.

Appendix A. Standard identities for Chebyshev polynomials

The following sets of equations are standard identities for Chebyshev polynomials.

$$\begin{aligned} \xi T_0(\xi) &= T_1(\xi) \\ 2\xi T_n(\xi) &= T_{n-1}(\xi) + T_{n+1}(\xi) \text{ for } n \geq 1 \end{aligned} \tag{34a}$$

$$\begin{aligned} 2\xi^2 T_0(\xi) &= T_0(\xi) + T_2(\xi) \\ 4\xi^2 T_1(\xi) &= 3T_1(\xi) + T_3(\xi) \\ 4\xi^2 T_n(\xi) &= T_{n-2}(\xi) + 2T_n(\xi) + T_{n+2}(\xi) \text{ for } n \geq 2 \end{aligned} \tag{34b}$$

$$\begin{aligned} T_0(\xi) &= T_1'(\xi) \\ T_1(\xi) &= \frac{1}{4} T_2'(\xi) \\ T_n(\xi) &= \frac{T_{n+1}'(\xi)}{2(n+1)} - \frac{T_{n-1}'(\xi)}{2(n-1)} \text{ for } n \geq 2 \end{aligned} \tag{34c}$$

$$\begin{aligned} T_0(\xi) &= \frac{1}{4} T_2''(\xi) \\ T_1(\xi) &= \frac{1}{24} T_3''(\xi) \\ T_2(\xi) &= \frac{1}{48} T_4''(\xi) - \frac{1}{6} T_2''(\xi) \\ T_n(\xi) &= \frac{T_{n+2}''(\xi)}{4(n+1)(n+2)} - \frac{T_n''(\xi)}{2(n^2-1)} + \frac{T_{n-2}''(\xi)}{4(n-1)(n-2)} \text{ for } n \geq 3 \end{aligned} \tag{34d}$$

These sets of identities define the matrices in (4). Explicit expressions for the matrices A, $\mathsf{B}_{[1]}$, and $\mathsf{B}_{[2]}^2$ are given in Eqs. (25), (31), and (34) of [10] (as well as many other references). Equations (34a,34b) follow from Eqs. (A.8,A.9) in the appendix of [52], while Eqs. (34c,34d) follow from Eq. (A.17) of [52].

Appendix B. Lane-Emden solution for non-integer polytropic indices

This appendix describes generation of spherically symmetric stellar models for non-integer n. For the numerical experiments considered in Subsection 4.1.2, we have found it useful to generate a double-valued solution on the overlap of the two spherical shells which surround a star. Here we describe the means by which this has been achieved.

B.1. **Dimensionless problem.** Consider the *Lane-Emden* problem for $0 \leq n \leq 5$,

$$\frac{d}{d\xi}\Big(\xi^2 \frac{d\theta}{d\xi}\Big) + \xi^2 \theta^n = 0, \qquad \theta(0) = 1, \quad \theta'(0) = 0. \tag{35}$$

Exact solutions are the following:

$$(n=0)\ \theta(\xi) = 1 - \tfrac{1}{6}\xi^2; \quad (n=1)\ \theta(\xi) = \xi^{-1}\sin(\xi); \quad (n=5)\ \theta(\xi) = \big(1 + \tfrac{1}{3}\xi^2\big)^{-1/2}. \tag{36}$$

We are most interested in the n-dependent root $\xi_\star$ at which $\theta(\xi_\star) = 0$, as well as the n-dependent number

$$\mu_\star := -\xi_\star \theta'(\xi_\star) \geq 0. \tag{37}$$

Exact cases are the following:

$$(n = 0)\ \xi_\star = \sqrt{6}, \mu_\star = 2; \quad (n = 1)\ \xi_\star = \pi, \mu_\star = 1; \quad (n = 5)\ \xi_\star = \infty, \mu_\star = 0. \tag{38}$$

B.2. **Physical variables.** Consider the polytropic equation of state

$$h = (n + 1)K\rho^{1/n}, \quad n > 0, \tag{39}$$

where both the enthalpy $h = h(r)$ and the density $\rho = \rho(r)$ are radial functions. The case $n = 0$ is special, with $\rho(r) = \rho_c$ (constant) and the enthalpy h not explicitly determined by ρ. The relationships between the Lane-Emden solution θ and the density and enthalpy are

$$\rho(r) = \rho_c \theta^n(r/\alpha), \qquad h(r) = \begin{cases} (n+1)K\rho_c^{1/n}\theta(r/\alpha) & \text{for } n > 0 \\ K\theta(r/\alpha) & \text{for } n = 0, \end{cases} \tag{40}$$

where the positive factor $\alpha = \alpha(n)$ is defined by

$$\alpha^2 := \begin{cases} (n+1)K\rho_c^{-1+1/n}/(4\pi G) & \text{for } n > 0 \\ K\rho_c^{-1}/(4\pi G) & \text{for } n = 0. \end{cases} \tag{41}$$

If the physical stellar radius $r = R$ is viewed as chosen, then $\alpha = R/\xi_\star$ and (41) determines the constant K appearing in (39).

Write the Lane-Emden equation as

$$-\frac{1}{r^2}\frac{d}{dr}\Big[r^2\frac{d}{dr}\Big(4\pi G\alpha^2\rho_c\theta\Big)\Big] = 4\pi G\rho_c\theta^n, \tag{42}$$

and view it as holding on $[0, R] = \alpha[0, \xi_\star]$. The interior ($r < R$) and exterior ($r > R$) gravitational potential $\Phi(r)$ are then

$$\Phi_{\rm int}(r) = -4\pi G\alpha^2\rho_c\big[C_1 + \theta(r/\alpha)\big], \quad \Phi_{\rm ext}(r) = -4\pi G\alpha^2\rho_c C_2/r, \tag{43}$$

where the constants [cf. (37) above]

$$C_1 = -\xi_\star\theta'(\xi_\star) = \mu_\star, \qquad C_2 = -\alpha\xi_\star^2\theta'(\xi_\star) = R\mu_\star \tag{44}$$

are determined by the matching conditions

$$\Phi_{\rm int}(R) = \Phi_{\rm ext}(R), \qquad \Phi'_{\rm int}(R) = \Phi'_{\rm ext}(R). \tag{45}$$

With (40) and (41), the first equation in (43) may then be written as

$$\Phi_{\rm int}(r) = -4\pi G\alpha^2\rho_c\mu_\star - h(r), \tag{46}$$

giving $\kappa = -4\pi G\alpha^2\rho_c\mu_\star$. Whence $\kappa = -(n+1)K\rho_c^{1/n}\mu_\star$ for $n > 0$ and $\kappa = -2K$ for $n = 0$.

The mass of the star is

$$M = 4\pi\int_0^R dr r^2\rho(r) = 4\pi\alpha^3\rho_c\int_0^{\xi_\star} d\xi\xi^2\theta^n(\xi) = \alpha^3\rho_c m_\star, \tag{47}$$

where the constant $m_\star$ may be computed via quadrature if θ is known. Exact cases are the following:

$$(n = 0)\ m_\star = \tfrac{1}{5}16\pi\sqrt{6}; \quad (n = 1)\ m_\star = 4\pi^2; \quad (n = 5)\ m_\star = \infty. \tag{48}$$

B.3. **Numerical solution.** If an analytic solution is not available for a given n, we begin by numerical computing the numbers $\xi_\star$ and $\mu_\star$. To achieve numerical approximations to these numbers which are accurate (in a relative sense) to machine double precision, we proceed as follows. As an initial value problem, we integrate (35) using a quadruple precision implementation of the 13-stage Dormand-Prince scheme. This integration relies on the scheme's 7th order embedded method to control the error through adaptive step size. The integration continues while $\theta > 0$ until $\theta = 0$ is achieved (to a sufficient tolerance).

Next, we use $\xi_\star$ and $\mu_\star$ to solve two problems via the modal-tau methods described in Section 2; for both problems writing the Lane-Emden equation as

$$\frac{d^2}{d\xi^2}\big(\xi^2\theta\big) - 2\frac{d}{d\xi}\big(\xi\theta\big) + \xi^2\theta^n = 0. \tag{49}$$

The first problem is posed on $[0, \xi_\star]$, and its solution is a Chebyshev spectrum $\widetilde{\boldsymbol{\theta}}^1$ labelled with a 1. Upon discretization, the first problem reads

$$I_{[2]}A_\xi^2\widetilde{\boldsymbol{\theta}}^1 - 2B_{\xi[2]}A_\xi\widetilde{\boldsymbol{\theta}}^1 + B_{\xi[2]}^2A_\xi^2\mathcal{F}\big[\big(\mathcal{F}^{-1}\widetilde{\boldsymbol{\theta}}^1\big)^n\big] = 0; \quad \boldsymbol{\delta}^-\widetilde{\boldsymbol{\theta}}^1 = 1, \quad \boldsymbol{\delta}^+\widetilde{\boldsymbol{\theta}}^1 = 0, \tag{50}$$

where $\mathcal{F}$ denotes the discrete Chebyshev transform and $\boldsymbol{\delta}^\pm$ are end-point Dirichlet vectors (comprised entirely of either ± 1 or 1). We solve this problem via Newton's method. Despite the potential loss of regularity in θ^n at the left endpoint, we are able to achieve a solution $\widetilde{\boldsymbol{\theta}}^1$ with near double precision accuracy, provided a sufficiently large truncation. Accuracy has been determined via comparison of $-\xi_\star\boldsymbol{\nu}^+\widetilde{\boldsymbol{\theta}}^1$ against the precomputed $\mu_\star$.

Although not necessary, it has proved convenient to also extend the *interior* density and gravitational potential beyond $r > R$, tantamount to extending $\theta(\xi)$ beyond $\xi > \xi_\star$. To achieve the extension, we pick $\xi_{\max} > \xi_\star$, and consider a second problem posed on $[\xi_\star, \xi_{\max}]$. The solution $\widetilde{\boldsymbol{\theta}}^2$ to the second problem is a Chebyshev spectrum labelled with a 2, and the second problem reads

$$I_{[2]}A_\xi^2\widetilde{\boldsymbol{\theta}}^2 - 2B_{\xi[2]}A_\xi\widetilde{\boldsymbol{\theta}}^2 + B_{\xi[2]}^2A_\xi^2\mathcal{F}\big[q\big|\mathcal{F}^{-1}\widetilde{\boldsymbol{\theta}}^2\big|^n\big] = 0; \quad \boldsymbol{\delta}^-\widetilde{\boldsymbol{\theta}}^2 = 0, \quad \boldsymbol{\nu}^-\widetilde{\boldsymbol{\theta}}^2 = -\mu_\star/\xi_\star, \tag{51}$$

where we may choose either $q = \pm 1$ or $q = 0$ (with $q = 1$ and no absolute value if n is integer). This choice affects how the solution is extended, and for the experiments in Subsection 4.1.2 this choice must be consistent with how the density is recovered in Subsection 3.4.2. We take $\rho_{\text{int}}(r) = \rho_c\theta^n(r/\alpha)$ and $\Phi_{\text{int}}(r)$ as the first formula in (43). We then use $\widetilde{\boldsymbol{\theta}}^1$ for evaluations of the interior solution when $r < R$, and $\widetilde{\boldsymbol{\theta}}^2$ for evaluations when $r > R$.

Appendix C. Matching conditions across a nonspherical stellar surface

Each step of our iterative approach (see below) involves update of the enthalpy h through Eq. (19b). We perform this update only on the inner region (shell 1 + block), and it yields (modal coefficients for) the updated density h^1. This enthalpy is smooth and defined everywhere on the inner region. Moreover, $h^1(\mathbf{x}) < 0$ outside of the current nonspherical surface ∂U. On the external region (shell 2) we demand $h^2(\mathbf{x}) = 0$ for all points.

Algorithm 3 COMPUTATION OF MATCHING CONDITIONS ACROSS A STELLAR SURFACE. Inputs are the modal coefficients $\{\widetilde{h}^1_{\ell qn}\}$ determining enthalpy $h^1(\mathbf{x})$ on shell 1. Outputs are the matrices $\widetilde{E}_{1,1:2}$ and $\widetilde{F}_{2,1:2}$ defining matching tau conditions.

1: Find surface ∂U on which $h^1 = 0$. Precisely, for each angular collocation direction (θ_j, ϕ_k) compute radius $r_{jk} = r(\theta_j, \phi_k)$ corresponding to $h^1(\mathbf{x}_{jk}) = 0$.

2: Using the spherical harmonic transform, from the r_{jk} obtain the modal coefficients $\widetilde{r}_{\ell m}$ which define the stellar surface ∂U as $r(\theta, \phi) = \sum_{\ell m} \widetilde{r}_{\ell m} Y_{\ell m}(\theta, \phi)$.

3: Obtain the components $\mathbf{n} = (n^1, n^2, n^3)$ of the normal to ∂U. Here we use

$$(1 - u^2)\frac{dP^m_\ell}{du} = (\ell + 1)uP^m_\ell - (\ell - m + 1)P^m_{\ell+1},$$

where $P^m_\ell(u)$ is an associated Legendre function with $u = \cos\theta$. This identity determines $\partial Y_{\ell m}/\partial x^k$ for $x^k = (x, y, z)$. Then $n^k \propto r^{-1}x^k - \sum_{\ell m} \widetilde{r}_{\ell m} \partial Y_{\ell m}/\partial x^k$.

4: For each shell $a = 1, 2$ compute and store the factors

$$\mathcal{E}^a_{\ell qn}(\mathbf{x}_{jk}), \qquad \mathcal{F}^a_{\ell qn}(\mathbf{x}_{jk}).$$

The angular factors defining these expressions may be computed once and stored. This step and the previous one defines the matrices $E_{1,1:2}$ and $F_{2,1:2}$.

5: Compute column-by-column spherical harmonic transforms $\widetilde{E}_{1,1:2}$ and $\widetilde{F}_{2,1:2}$.

On shell $a = 1, 2$ the coefficients $\widetilde{\Phi}^a_{\ell qn}$ determine the function (cf. Eq. (15) of [11])

$$\mathcal{P}_{N^a_r, N_\theta}\Phi^a(r, \theta, \phi) = \sum_{\ell=0}^{N_\theta} \sum_{q=0}^{2N_\theta} \sum_{n=0}^{N^a_r} \widetilde{\Phi}^a_{\ell qn} \mathcal{E}^a_{\ell qn}(r, \theta, \phi). \tag{52}$$

Here the $\mathcal{P}$ merely indicates that the function arises as a finite expansion. Moreover, the basis functions $\mathcal{E}^a_{\ell qn}(r, \theta, \phi)$ are (with $m = 1, \ldots, N_\theta$)

$$\begin{aligned} \mathcal{E}^a_{\ell 0n}(r, \theta, \phi) &= \overline{P}_{\ell 0}(\cos\theta) T_n(\xi^a(r)) \\ \mathcal{E}^a_{\ell, 2m-1, n}(r, \theta, \phi) &= \overline{P}_{\ell m}(\cos\theta)\cos(m\phi) T_n(\xi^a(r)) \\ \mathcal{E}^a_{\ell, 2m, n}(r, \theta, \phi) &= \overline{P}_{\ell m}(\cos\theta)\sin(m\phi) T_n(\xi^a(r)), \end{aligned} \tag{53}$$

where the $\overline{P}_{\ell m}(u)$ are normalized associated Legendre functions (denoted by $\overline{P}^m_\ell(u)$ in Ref. [53]) and $\xi^a(r)$ maps the shell-a radial domain $[r^a_{\min}, r^a_{\max}]$ to $[-1, 1]$.

Conditions which enforce continuity of the numerical solution and its normal derivative across the stellar surface ∂U are then represented by

$$\mathcal{P}_{N^1_r, N_\theta}\Phi^1(\mathbf{x}_{jk}) = \mathcal{P}_{N^2_r, N_\theta}\Phi^2(\mathbf{x}_{jk}),\ \mathbf{n} \cdot \big(\nabla\mathcal{P}_{N^1_r, N_\theta}\Phi^1\big)(\mathbf{x}_{jk}) = \mathbf{n} \cdot \big(\nabla\mathcal{P}_{N^2_r, N_\theta}\Phi^2\big)(\mathbf{x}_{jk}), \tag{54}$$

where $\mathbf{x}_{jk} = \mathbf{x}(r_{jk}, \theta_j, \phi_k)$ are Cartesian points on and $\mathbf{n}$ is the normal to ∂U. In practice the points $\mathbf{x}_{jk}$ are determined by the angular collocation points (θ_j, ϕ_k) corresponding the (discrete) spherical harmonic transform [54] and the corresponding radial values r_{jk}. The preceding equations determine $2(N_\theta + 1)(2N_\theta + 1)$ linear relationships between the modal coefficients $\widetilde{\Phi}^1_{\ell qn}$ and $\widetilde{\Phi}^2_{\ell qn}$. Indeed, there are $(N_\theta + 1)(2N_\theta + 1)$ physical points $\mathbf{x}_{jk}$. Among these relationships are, for example,

$$\sum_{\ell=0}^{N_\theta} \sum_{q=0}^{2N_\theta} \sum_{n=0}^{N^1_r} \widetilde{\Phi}^1_{\ell qn} \mathcal{F}^1_{\ell qn}(\mathbf{x}_{jk}) = \sum_{\ell=0}^{N_\theta} \sum_{q=0}^{2N_\theta} \sum_{n=0}^{N^2_r} \widetilde{\Phi}^2_{\ell qn} \mathcal{F}^2_{\ell qn}(\mathbf{x}_{jk}), \tag{55}$$

where $\mathcal{F}^a_{\ell qn}(\mathbf{x}) \equiv (\mathbf{n}\cdot\nabla\mathcal{E}^a_{\ell qn})(\mathbf{x})$. Evidently, this is a linear relationship expressible in terms of the vector direct sum of the modal coefficients $\widetilde{\Phi}^1_{\ell qn}$ and $\widetilde{\Phi}^2_{\ell qn}$ as well as a matrix $F_{2,1:2}$ which has $\mathcal{F}^1_{\ell qn}(\mathbf{x}_{jk})$ and $\mathcal{F}^2_{\ell qn}(\mathbf{x}_{jk})$ as entries. The lead index 2 on $F_{2,1:2}$ indicates that these relationships as intended for filling zero rows associated with the shell 2 row sector of the linear system, and the trailing 1:2 (colon notation) that they will stretch across the shell 1 and shell 2 column sectors. The other set of matching conditions similarly determine a matrix $E_{1,1:2}$.

The matrices $E_{1,1:2}$ and $F_{2,1:2}$ have too many rows, since, as mentioned above, there are only $2(N_\theta+1)^2$ free rows of zeros, whereas both $E_{1,1:2}$ and $F_{2,1:2}$ have $(N_\theta+1)(2N_\theta+1)$ rows. We reduce the number of equations as follows. Using the spherical harmonic transform, we compute the column-by-column transforms $\widetilde{E}_{1,1:2}$ and $\widetilde{F}_{2,1:2}$. The rows of these matrices which correspond to physical index pairs then define the tau conditions. The procedure is summarized in Algorithm I.

Appendix D. Hachisu regularization for non-equal masses

Reference [7] has described Hachisu regularization of the SCF method for non-equal masses. However, that reference considers only a white-dwarf EOS, and not the polytropic EOS considered in this paper. We extend the procedure of [7] to the polytropic EOS. For the non-equal mass Hachisu regularization (as with Meudon regularization), in line 8 of **Algorithm 2** we enforce symmetry across the $x = 0$ and $y = 0$ coordinate planes. The SCF update of the enthalpy is performed via the same Hachisu approach described in Subsection 3.4. Therefore, what remains unspecified are the auxiliary equations determining the parameters κ_I, κ_{II}, Ω^2, and ℓ_z.

The auxiliary equations are determined as follows. First, we fix the z-extents of star I through $z_A \le z \le z_B$, as before. We also then fix the inner extent of star II through $0 < z_C \le z$. Through the generalized potential equation these three conditions yield the first three equations. The fourth equation relates the maximum enthalpy value in each star. The auxiliary equations are then the following:

$$\kappa_I = \Phi_A - \tfrac{1}{2}(z_A - \ell_z)^2\Omega^2 \tag{56a}$$

$$\kappa_I = \Phi_B - \tfrac{1}{2}(z_B - \ell_z)^2\Omega^2 \tag{56b}$$

$$\kappa_{II} = \Phi_C - \tfrac{1}{2}(z_C - \ell_z)^2\Omega^2 \tag{56c}$$

$$\frac{K_I}{K_{II}}\Big(\frac{\rho_{\max,I}}{\rho_{\max,II}}\Big)^{1/n} = \frac{\big[\kappa_I - \Phi|_{\mathbf{x}_I} + \frac{1}{2}(z_I - \ell_z)^2\Omega^2\big]}{\big[\kappa_{II} - \Phi|_{\mathbf{x}_{II}} + \frac{1}{2}(z_{II} - \ell_z)^2\Omega^2\big]} \tag{56d}$$

As mentioned before, the locations $\mathbf{x}_{I,II} = (0, 0, z_{I,II})$ of the enthaply maxima are known to lie on the z-axis by symmetry, although the values $z_{I,II}$ are determined by a numerical search performed during each SCF step. Note that the expression on the left-hand side of (56d) is viewed as a fixed constant throughout the SCF iteration.

Appendix E. Computation of stellar integrals

To evaluate integrals such as (33), we have adopted a straightforward procedure, albeit one that leaves room for improvement. Consider star I for definiteness. A integral over this

star is first expressed as

$$\int_{\text{star } I} d\mathbf{x} f(\mathbf{x}) = \underbrace{\int_{|\mathbf{x}|\le r^1_{\min}} d\mathbf{x} f(\mathbf{x})}_{B^2 \text{ term}} + \underbrace{\int_0^{2\pi} d\phi \int_0^{\pi} d\theta \sin\theta \int_{r^1_{\max}}^{r_I(\boldsymbol{\theta})} dr r^2 f(r\boldsymbol{\theta})}_{S^1_I \text{ term}} . \tag{57}$$

The "B^2 term" must be computed from the modal expansion coefficients for the function f on B^2. We approximate this integral with Stroud's fifth degree rule for a ball; see **Formula I** for $n = 3$ on page 92 of [55]. The "S^1_I term" must be computed from the modal expansion coefficients for the function f on S^1_I. We approximate this integral as follows. Let (θ_j, ϕ_k) represent the angular collocation points corresponding to the (discrete) spherical harmonic transform [54]. Then for each such point we evaluate $g_{jk} = g(\boldsymbol{\theta}_{jk})$, with the integral

$$g(\boldsymbol{\theta}) := \int_{r^1_{\max}}^{r_I(\boldsymbol{\theta})} dr r^2 f(r\boldsymbol{\theta}) \tag{58}$$

computed via composite Gauss-Kronrod quadrature. Upon spherical harmonic transformation of g, we isolate the $(\ell = 0, q = 0)$ modal coefficient $\widetilde{f}_{00}$. The expression $2\sqrt{2}\pi\widetilde{f}_{00}$ is then the second integral in question.

References

[1] J. W. York, Jr., *Kinematics and Dynamics of General Relativity* in *Sources of gravitational radiation: Proceedings of Battelle Seattle Workshop, July 24 - August 4, 1978*, ed. L. L. Smarr (Cambridge University Press, Cambridge, 1979).

[2] J. M. Bowen and J. W. York, Jr., *Time-asymmetric initial data for black holes and black-hole collisions*, Phys. Rev. D 21 (1980) 2047-2056.

[3] J. W. York, Jr., *Conformal "Thin-Sandwich" Data for the Initial-Value Problem of General Relativity*, Phys. Rev. Lett. 82 (1999) 1350-1353.

[4] H. P. Pfeiffer and J. W. York, Jr., *Extrinsic curvature and the Einstein constraints*, Phys. Rev. D 67, 044022 (2003) [8 pages].

[5] I. Hachisu, *A versatile method for obtaining structures of rapidly rotating stars*, Astrophys. J. Supp. Series 61 (1986) 479-507.

[6] I. Hachisu, *A versatile method for obtaining structures of rapidly rotating stars. II. Three-dimensional self-consistent field method*, Astrophys. J. Supp. Series 62 (1986) 461-499.

[7] I. Hachisu, Y. Eriguchi, and K. Nomoto, *Fate of merging double white dwarfs. II. Numerical method*, Astrophys. J. 311 (1986) 214-225.

[8] K. Taniguchi and E. Gourgoulhon, *Equilibrium sequences of synchronized and irrotational binary systems composed of different mass stars in Newtonian gravity*, Phys. Rev. D 65 (2002) 044027 [16 pages].

[9] S. R. Lau and R. H. Price, *Sparse Modal Tau-Method for Helical Binary Neutron Stars*, Lecture Notes in Computational Science and Engineering 106 (2015) 315-323. Proceedings of Spectral and High Order Methods for Partial Differential Equations ICOSAHOM 2014.

[10] S. R. Lau and R. H. Price, *Multidomain Spectral Method for the Helically Reduced Wave Equation*, J. Comput. Phys. 227(2) (2007) 1126-1161. We regret an error in the definition of ν^- in Eq. (42). The correct expressions are $\nu^{\pm} = [T'_0(\pm1), T'_1(\pm1), T'_2(\pm1), T'_3(\pm1), T'_4(\pm1), \cdots] = [0, 1, \pm4, 9, \pm16, \cdots]$. The right-hand side of the second equation of (69) is also off by a sign.

[11] S. R. Lau and R. H. Price, *Sparse spectral-tau method for the three-dimensional helically reduced wave equation on two-center domains*, J. Comput. Phys. 231(2) (2012) 7695-7714.

[12] M. Beroiz, T. Hagstrom, S. R. Lau, and R. H. Price, *Multidomain, sparse, spectral-tau method for helically symmetric flow*, Computers & Fluids 102 (2014) 250-265.

[13] J. Eggers and M. A. Fontelos, *Singularities: Formation, Structure, and Propagation* (Cambridge University Press, Cambridge, 2015)

[14] L. Bourouiba, J. W. M. Bush, *Drops and Bubbles in the Environment*, Chapter 32 in *Handbook of Environmental Fluid Dynamics, Overview and Fundamentals, Volume One*, edited by H. J. S. Fernando (CRC Press, Taylor & Francis Group, Boca Raton, 2013). https://doi.org/10.1201/b14241
[15] C. Pozrikidis, *Interfacial Dynamics for Stokes Flow*, J. Comput. Phys. 169(2) (2001) 250-301.
[16] D. Crowdy and M. Siegel, *Exact solutions for the evolution of a bubble in Stokes flow: a Cauchy transform approach*, SIAM J. Appl. Math. 65(3) (2005) 941-963.
[17] R. Ojala and A.-K. Tornberg, *An accurate integral equation method for simulating multi-phase Stokes flow*, J. Comput. Phys. 298(1) (2015) 145-160.
[18] R. Glowinski, T. W. Pan, J. Periaux, *Fictitious Domain/Domain Decomposition Methods for Partial Differential Equations*, pp. 177-192 and Chapter 11 of *Domain-Based Parallelism and Problem Decomposition Methods in Computational Science and Engineering*, edited by D. E. Keyes, Y. Saad, and D. G. Truhlar (SIAM, Philadelphia, 1995).
[19] A. McKenney, L. Greengard, A. Mayo, *A fast Poisson solver for complex geometries*, J. Comput. Phys 118(2) (1995) 348-355.
[20] A. Greenbaum and A. Mayo, *Rapid Parallel Evaluation of Integrals in Potential Theory on General Three-Dimensional Regions*, J. Comput. Phys. 145(2) (1998) 731-742.
[21] A. Mayo and A. Greenbaum, *Fourth order accurate evaluation of integrals in potential theory on exterior 3D regions*, J. Comput. Phys. 220(2) (2007) 900-914.
[22] R. J. LeVeque and Z. Li, *Immersed Interface Methods for Stokes Flow with Elastic Boundaries or Surface Tension*, SIAM J. Sci. Comput. 18(3) (1997) 709-735.
[23] Z. Li and K. Ito, *The Immersed Interface Method – Numerical Solutions of PDEs Involving Interfaces and Irregular Domains*, SIAM Frontiers in Applied Mathematics 33 (SIAM, Philadelphia, 2006),
[24] A. N. Marquesa, J.-C. Nave, R. R. Rosalesc, *High order solution of Poisson problems with piecewise constant coefficients and interface jumps*, J. Comput. Phys. 335 (2017) 497-515.
[25] S. Bonazzola, E. Gourgoulhon, and J.-A. Marck, *Relativistic formalism to compute quasiequilibrium configurations of nonsynchronized neutron star binaries*, Phys. Rev. D 56 (1997) 7740-7749.
[26] S. Bonazzola, E. Gourgoulhon, and J.-A. Marck, *Numerical Models of Irrotational Binary Neutron Stars in General Relativity*, Phys. Rev. Lett. 82, 892-895 (1999).
[27] E. Gourgoulhon, P. Grandclément, K. Taniguchi, J.-A. Marck, and S. Bonazzola, *Quasiequilibrium sequences of synchronized and irrotational binary neutron stars in general relativity: Method and tests*, Phys. Rev. D 63, 064029 (2001) [27 pages].
[28] T. Dietrich, N. Moldenhauer, N. K. Johnson-McDaniel, S. Bernuzzi, C. M. Markakis, B. Brügmann, and W. Tichy, *Binary neutron stars with generic spin, eccentricity, mass ratio, and compactness: Quasi-equilibrium sequences and first evolutions*, Phys. Rev. D 92, 124007 (2015) [39 pages].
[29] W. E. East, F. M. Ramazanoğlu, and F. Pretorius, *Conformal thin-sandwich solver for generic initial data*, Phys. Rev. D 86, 104053 (2012) [12 pages].
[30] N. Moldenhauer, C. M. Markakis, N. K. Johnson-McDaniel, W. Tichy, B. Brügmann, *Initial data for binary neutron stars with adjustable eccentricity*, Phys. Rev. D 90, 084043 (2014) [23 pages].
[31] A. Tsokaros, K. Uryu, and L. Rezzolla, *New code for quasiequilibrium initial data of binary neutron stars: Corotating, irrotational, and slowly spinning systems*, Phys. Rev. D 91, 104030 (2015) [29 pages].
[32] S. Bonazzola, J. Frieben, E. Gourgoulhon, and J.-A. Marck, *Spectral methods in general relativity — towards the simulation of 3D-gravitational collapse of neutron stars*, Spec. Issue Houston Journal of Mathematics (1996) 3-19.
[33] E. A. Coutsias, T. Hagstrom, J. S. Hesthaven, and D. Torres, *Integration preconditioners for differential operators in spectral τ-methods*, Spec. Issue Houston Journal of Mathematics (1996) 21-38.
[34] E. Gourgoulhon, P. Grandclément, J.-A. Marck, J. Novak, and K. Taniguchi, http://www.lorene.obspm.fr.
[35] https://www.black-holes.org
[36] Spectral Einstein Code (SpEC): http://www.black-holes.org/SpEC.html
[37] H. P. Pfeiffer, L. E. Kidder, M. A. Scheel, and S. A. Teukolsky, *A multidomain spectral method for solving elliptic equations*, Comput. Phys. Commun. 152(3) (2003) 253-273.
[38] F. Foucart, L. E. Kidder, H. P. Pfeiffer, and S. A. Teukolsky, *Initial data for black hole-neutron star binaries: A flexible, high-accuracy spectral method* Phys. Rev. D 77, 124051 (2008) [20 pages].

[39] H. Pfeiffer, N. Tacik, F. Foucart, R. Haas, J. Kaplan, C. Muhlberger M. Duez, L. Kidder, M. Scheel, and B. Szilagyi, *Abstract: Y13.00004 : Binary Neutron Stars with Arbitrary Spins in Numerical Relativity*, APS April Meeting 2015, `http://meetings.aps.org/link/BAPS.2015.APR.Y13.4`.
[40] K. Henriksson, F. Foucart, L. E. Kidder, and S. A. Teukolsky, *Initial data for high-compactness black hole-neutron star binaries*, Class. Quantum Grav. 33, 105009 (2016) [22 pages].
[41] W. Tichy, *A new numerical method to construct binary neutron star initial data*, Class. Quantum Grav. 26, 175018 (2009) [15 pages].
[42] W. Tichy, *Constructing quasi-equilibrium initial data for binary neutron stars with arbitrary spins*, Phys. Rev. D 86, 064024 (2012) [8 pages].
[43] M. Ansorg, *Multi-domain spectral method for initial data of arbitrary binaries in general relativity*, Class. Quantum Grav. 24 (2007) S1-14.
[44] C. W. Misner, K. S. Thorne, and J. A. Wheeler, *Gravitation* (Freeman, San Francisco, 1973).
[45] E. A. Coutsias, T. Hagstrom, and D. Torres, *An efficient spectral method for ordinary differential equations with rational function coefficients*, Math. Comput. 65(214) (1996) 611-635.
[46] J. P. Ostriker and J. W.-K. Mark, Astrophys. J. 151 (1968) 1075-1088.
[47] S. Bonazzola, E. Gourgoulhon, and J.-A. Marck, *Numerical approach for high precision 3D relativistic star models* Phys. Rev. D 58, 104020 (1998) [14 pages].
[48] S. Chandrasekhar, *An Introduction to the Study of Stellar Structure* (Dover Publishing Inc., New York, 1967).
[49] S. R. Lau and R. H. Price, *Helically reduced wave equations and binary neutron stars*, to appear in *Lecture Notes in Computational Science and Engineering*. Proceedings of Spectral and High Order Methods for Partial Differential Equations ICOSAHOM 2016.
[50] C. T. Kelley, *Iterative Methods for Linear and Nonlinear Equations* (SIAM, Philadelphia, 1995).
[51] S. R. Lau, *Second-order formalism for helically symmetric spacetimes describing binary neutron stars*, in preparation, Summer 2017.
[52] J. P. Boyd, *Chebyshev and Fourier Spectral Methods*, second edition (Dover Publishing Inc., New York, 2001).
[53] M. Abramowitz and I. A. Stegun, *Handbook of Mathematical Functions* (Dover Publishing Inc., New York, 1970).
[54] J. C. Adams and P. N. Swarztrauber, *SPHEREPACK 3.0: A Model Development Facility*, Mon. Wea. Rev. 127 (1999) 1872-1878.
[55] A. H. Stroud, *Some Fifth Degree Integration Formulas for Symmetric Regions*, Math. Comp. 20 (93) (1966) 90-97.

(S. R. Lau) Department of Mathematics and Statistics, 1 University of New Mexico, Albuquerque, NM 87131